Emulsion characterization via microfluidic devices : A review on interfacial tension and stability to coalescence

Ho, Minh Thao

2022-01

Ho , M T , Aysan , R , Ramachandran , A & Mikkonen , K S 2022 , ' Emulsion characterization via microfluidic devices : A review on interfacial tension and stability to coalescence ' , Advances in Colloid and Interface Science , vol. 299 , 102541 . https://doi.org/10.1016/j.cis.2021.102

http://hdl.handle.net/10138/339366
https://doi.org/10.1016/j.cis.2021.102541

Advances in Colloid and Interface Science 299 (2022) 102541

Contents lists available at ScienceDirect

Advances in Colloid and Interface Science

journal homepage: www.elsevier.com/locate/cis

Historical Perspective

Emulsion characterization via microfluidic devices: A review on interfacial tension and stability to coalescence

Thao Minh Ho [a,b,*], Aysan Razzaghi [c], Arun Ramachandran [c], Kirsi S. Mikkonen [a,b]

[a] Department of Food and Nutrition, P.O. Box 66, 00014, University of Helsinki, Finland
[b] Helsinki Institute of Sustainability Science (HELSUS), P.O. Box 65, 00014, University of Helsinki, Finland
[c] Department of Chemical Engineering and Applied Chemistry, University of Toronto, 200 College Street, Toronto, ON M5S 3E5, Canada

ARTICLE INFO

Keywords:
Emulsion
Interfacial tension
Microfluidic device
Coalescence
Emulsion stability

ABSTRACT

Emulsions have gained significant importance in many industries including foods, pharmaceuticals, cosmetics, health care formulations, paints, polymer blends and oils. During emulsion generation, collisions can occur between newly-generated droplets, which may lead to coalescence between the droplets. The extent of coalescence is driven by the properties of the dispersed and continuous phases (e.g. density, viscosity, ion strength and pH), and system conditions (e.g. temperature, pressure or any external applied forces). In addition, the diffusion and adsorption behaviors of emulsifiers which govern the dynamic interfacial tension of the forming droplets, the surface potential, and the duration and frequency of the droplet collisions, contribute to the overall rate of coalescence. An understanding of these complex behaviors, particularly those of interfacial tension and droplet coalescence during emulsion generation, is critical for the design of an emulsion with desirable properties, and for the optimization of the processing conditions. However, in many cases, the time scales over which these phenomena occur are extremely short, typically a fraction of a second, which makes their accurate determination by conventional analytical methods extremely challenging. In the past few years, with advances in microfluidic technology, many attempts have demonstrated that microfluidic systems, characterized by micrometer-size channels, can be successfully employed to precisely characterize these properties of emulsions. In this review, current applications of microfluidic devices to determine the equilibrium and dynamic interfacial tension during droplet formation, and to investigate the coalescence stability of dispersed droplets applicable to the processing and storage of emulsions, are discussed.

1. Introduction

Emulsions are colloidal dispersions composed of two immiscible liquids, typically oil and water, that contain dispersed droplets with a mean diameter usually in the range of 0.1–100 μm [1]. Based on the droplet size distribution, characterized by uniformity or coefficient of variation (CV) value, emulsions are typically considered as "monodisperse" when their CV values are smaller than 25% [2]. Monodisperse emulsions have gained special attention in many research fields and industries. In the pharmaceutical industry, designing drug delivery systems with small drop sizes and narrow size distributions is essential to avoid variabilities in drug release behaviors and to prevent the accumulation of the microspheres at undesirable locations in the body [3]. In the construction industry, the use of adhesive agents in the form of a solution, emulsion, or dispersion (in a solvent such as water, alcohol, or hydrocarbons) with monodisperse particles for the insulation in buildings is also preferred as they provide good bonding strength [4]. In the food industry, the production of monodisperse emulsions is being considered as a new and emerging technology to protect and control the release rate of many important bioactive compounds [5]. Having a tight size distribution is also desirable as it mitigates Ostwald ripening by reducing the effective Laplace pressure difference that drives mass transfer [6]. With rapid advances in microfluidic technology, many approaches have been proposed to prepare highly monodisperse emulsions, but their low throughput has limited them from advancing to industrial scale production. Meanwhile, the production of monodisperse emulsions using microfluidic devices at small scales (e.g. laboratory scale) has resulted in a large number of studies in various fields, and many excellent reviews, including for food applications, have been reported [7–17].

* Corresponding author at: Department of Food and Nutrition, P.O. Box 66, 00014, University of Helsinki, Finland.
E-mail address: minh.ho@helsinki.fi (T.M. Ho).

https://doi.org/10.1016/j.cis.2021.102541
Received in revised form 22 September 2021;
Available online 5 October 2021

Emulsions are prone to thermodynamically favorable phase separation during storage. The phase separation can be retarded by adding suitable stabilizers during emulsion preparation. The stabilizers can either be thickening agents that increase the viscosity of the continuous phase, thereby delaying coalescence and phase separation, or emulsifiers such as amphiphilic biopolymer molecules, low molecular weight surfactants and solid particles as in Pickering emulsions, which are able to adsorb to the interfacial regions to cause a repulsive disjoining pressure barrier to coalescence [18]. During emulsification, two competing processes happen simultaneously, namely the disintegration of the dispersed phase to produce droplets, and the coalescence of the generated droplets; this could lead to a phenomenon known as "morphological hysteresis" in a mixing device [19]. To ensure that the droplet size distribution remains stable, the droplets need to be prevented from coalescing with each other, and the emulsifiers play this role. The presence of suitable emulsifiers lowers the interfacial tension between the continuous and dispersed phases, thus decreasing the energy required to form a new interface and facilitating the formation of droplets. Additionally, as mentioned above, the emulsifiers can provide an energy barrier against coalescence and confer a suitable lifetime for the final emulsified products [20–23]. Therefore, an understanding of rates of emulsifier adsorption and desorption processes on the interface is critical to manipulate and design the interface structure of emulsions for a particular application. Unfortunately, the time scales for these processes occurring on the interface during droplet formation (e.g. adsorption behaviors of emulsifiers and coalescence of the generated droplets) can be extremely short (from sub-milliseconds to milliseconds), and prior to the advent of microfluidics, there were no analytical methods that allowed us to accurately probe these phenomena at such small time scales. Apart from the preparation of monodisperse emulsions, many reported studies have demonstrated that microfluidic devices can be employed as an analytical platform to study the adsorption behaviors of emulsifiers during droplet generation and to determine their roles in the prevention of droplet coalescence. However, there is no comprehensive review dedicated to this aspect of microfluidic devices. This article aims to review fundamental aspects of emulsions, especially their instability mechanisms, and to describe existing microfluidic devices with different configurations and fabrication materials that can investigate emulsion-related properties. The applicability of microfluidic devices for determining interfacial tension (IFT) during the formation of dispersed droplets, and investigating the coalescence stability of dispersed droplets, are comprehensively discussed. Although most reported studies discussed in this review are not directly performed for food applications, they could be easily applied to food-grade emulsions due to similarities in the nature, properties and functions of emulsions in different fields.

2. Formation and stabilization of emulsions

Due to the importance of emulsions as a material class, many aspects of emulsions have been well documented and many comprehensive reviews on emulsions have been reported [1,24–29]. Therefore, the scope of this review is restricted to the fundamentals of the formation and stabilization of emulsions that are most relevant to emulsion characterization via microfluidic devices.

2.1. What is interfacial tension?

From a thermodynamic perspective, a mixture of two liquids separates into distinct phases, when the cohesive forces of interaction for the molecules of each phase exceed the adhesive forces of interaction between the two different liquid molecules. The interface between the two liquids, thus, represents a region where molecules of either phase ideally do not desire to reside, and as such, the energy per molecule for either liquid is greater at the interface compared to that of the bulk. Hence, when an emulsion is created, in many cases, the mixture is thermodynamically driven to reduce the interfacial area and therefore the total interfacial energy between the two phases. The interfacial tension is the increase in the excess energy per unit increase in area at the interface; the larger the interfacial tension, the greater the driving force to minimize the interfacial area.

The interfacial tension has a mechanical description as well. The interfacial tension γ (N/m) can be interpreted as the isotropic interfacial stress tensor acting at the interface between two immiscible fluids. An isotropic model of the interfacial stress tensor is able to quantitatively describe the interfacial stress tensor not only for clean (surfactant free) interfaces between simple fluids, but also in the presence of certain kinds of surfactants. However, for complex interfaces, due either to complex bulk fluids or to special interfacially active species, the interface could exhibit viscoelastic and other non-linear properties [30]. For such interfaces, more advanced constitutive models are required [31–34]. For the remainder of this review, we will focus on simple interfaces that can be described by an isotropic interfacial tension, for which the stress jump across the interface comprises two contributions. The first is the capillary stress or the Laplace pressure, which is proportional to the total local interfacial curvature and the interfacial tension, and produces a discontinuity in the bulk normal stresses exerted by the two fluids on the interface. The second contribution is called the Marangoni stress, and produces a jump in the tangential components of the bulk stresses due to the fluids on either side of the interface. Marangoni stresses are generated when there are gradients in interfacial tension due to variations in surfactant concentration or temperature along the interface, and drive interfacial motion from regions of low interfacial tension to high. They can play a key role in coalescence dynamics, as discussed later.

2.2. Hydrodynamic drop breakup

The interfacial tension plays a major role in the evolution of the interfacial area between the dispersed and continuous phases in a sheared emulsion, as it strongly affects the two major phenomena that impact drop size – drop breakup and droplet-droplet coalescence, which increase and reduce, respectively, the total interfacial area [19]. We will present here a brief review of hydrodynamic drop breakup mechanisms. A review of flow-induced coalescence phenomena is provided in section 4.2. For a drop in an emulsion, once the hydrodynamic stresses exerted on the drop by the continuous medium exceed the restoring stresses provided by interfacial tension, the drop undergoes a continuous deformation. To account for the balance between hydrodynamic and interfacial stresses, the literature has seen primarily two dimensionless groups. When the flow is dominated by viscous effects, the balance is captured by the capillary number (Ca), which is the ratio of the characteristic viscous stresses to interfacial stresses, and is defined as $\mathrm{Ca} = \mu GR/\gamma$. Here G is the local extensional rate experienced by the drop, μ is the viscosity of the suspending medium, and R is the drop radius. As shown in prior work [35–38] the critical capillary number for breakup depends on the drop to suspending medium viscosity ratio (λ), and also the nature of the flow (shear flow, purely extensional flow, etc.). For inertially-dominated flows, it is more appropriate to use a Weber number, $We = \rho U^2 R/\gamma$, which is the ratio of the characteristic inertial stresses in the flow to interfacial stresses. Here U is the characteristic velocity scale of the flow. The critical Weber number for breakup is written as a function of the Ohnesorge number [39], which is a dimensionless group that accounts for the effect of drop viscosity on breakup characteristics. When either the capillary number or the Weber number in the flow exceed their respective critical values, the drop experiences continuous stretching and forms ligaments. The ligaments can fragment into small droplets during the process of stretching via the onset of capillary instabilities. Alternatively, the stretched drop can experience a reduction in the extensional rate and/or a change in the nature of the flow, causing the drop to begin to relax back towards its initial, spherical shape. During the process of relaxation, the drop may undergo breakup via the end pinch and/or capillary instability mechanisms. The pinch point for

fragmentation, the number of drops produced, and their size distribution depend on the time history of the flow as well as the dispersed to continuous phase viscosity ratio [37]. Apart from the drop fracture mechanism of breakup outlined above, there are also secondary mechanisms of drop breakup. As a ligament of drop fluid undergoes fracture, it can form one or more generations of satellite droplets in between the daughter droplets. The satellite droplets can be several orders of magnitude smaller than the parent drop. Generally, satellite droplet formation is more prominent for emulsions where the drop viscosity is less than the medium viscosity. A second mechanism for secondary hydrodynamic breakup leading to the formation of extremely small droplets is tip streaming. In this phenomenon, a stream of the fragmented drops emerges from the tips of the sheared parent drop [40–48]. The presence of a surfactant is thought to be essential to observe tip streaming, and it is the local interfacial tension reduction produced by the accumulation of surfactant molecules at the stretched tips that leads to the phenomenon. The manifestation of tip streaming requires a delicate balance among the processes of surfactant adsorption-desorption kinetics, surfactant mass transfer, interfacial convection of the surfactant, and the decrease in interfacial tension with surfactant concentration [42,45]. In microfluidic applications where droplet production, interfacial tension measurement or coalescence studies are the focus, the experimental conditions (the surfactants, the two phases and the flow geometry) should be selected to minimize or avoid secondary mechanisms. For example, tip streaming is suppressed when $\lambda > 0.1$ [37,49] and when surfactant adsorption-desorption rates are high compared to the convective transport of the surfactant at the interface [43,44]. Moderate to high viscosity ratios also mitigate the formation of satellite drops [37]. Drops can also produce fine threads that break up into small droplets as they pass through constrictions or expansions in microfluidic channels [50], particularly at low viscosity ratios and low Ca numbers. The process of entering a constriction, for example, involves the front of the drop accelerating significantly more than the back, which can lead to the production of a thread in the rear. Similarly, as the drop exits a constricted section into an expansion, capillary forces can cause a sudden expansion and acceleration of the front of the drop relative to the rear, which can again produce a thread trailing the drop that disintegrates into fine droplets. To avoid break-up by this mechanism, the geometries of constrictions and expansions (taper angle and shape, contrast in upstream and downstream channel dimensions) need to be considered carefully in conjunction with the flow conditions and fluid properties [50].

2.3. The need for emulsifiers and their systematic selection

To synthesize an emulsion, mechanical shearing forces are typically employed to break the dispersed phase into very small droplets, leading to a substantial increase in the interfacial area. Adding interfacially active species termed as emulsifiers during the processing of emulsions is an effective approach to reduce IFT. Having both hydrophilic and hydrophobic groups in the structure provides emulsifiers with the ability to arrange and adsorb on the surfaces of the generated dispersed droplets. A key question is, what molecular structure of an emulsifier favours a reduction in the interfacial tension? A desirable emulsifier should reduce the interfacial tension considerably, but not to such an extent that the phase inversion point is reached or crossed. In general, a proper balance with respect to the hydrophilic and lipophilic properties of the surfactant system is required for an emulsifier to act effectively [51]. While there are several frameworks available to select surfactants, e.g. Bancroft's rule, the phase inversion point, packing parameter, hydrophilic- lipophilic balance (HLB), etc. [23,52–55], arguably, the most comprehensive framework available today to design surfactants for specific applications is the hydrophilic-lipophilic difference (HLD) model [22,23,56]. The drawback with past frameworks is that, when determining whether the surfactant leads to an oil-in-water (O/W) or a water-in-oil (W/O) emulsion, they are either too simplistic (e.g. Bancroft's rule), or consider the structure of a surfactant in isolation (e.g. HLB), or involve parameters that are difficult to measure (e.g. packing parameter). However, practically, the outcome also depends on the chemistries of the oil and aqueous phases, the salinity in the aqueous phase, and the temperature. The HLD model accounts for all of these variables with a single equation, as HLD is a measure of the difference between the chemical potentials of an emulsifier molecule in the oil phase and the aqueous phase. Negative values of HLD indicate that the combination of emulsifier, water and oil will lead to an O/W emulsion, while positive HLD values imply that the emulsifier will produce a W/O emulsion.

The equations used in the HLD model are as follows [57,58,60]:

For ionic surfactants $\mathrm{HLD} = \ln(S) - K \times \mathrm{EACN} + \sigma + a f(\mathrm{A}) - a_T(T - 25)$.

For nonionic surfactants $\mathrm{HLD} = bS - K \times \mathrm{EACN} + \beta + a\,\varphi(\mathrm{A}) + c_T(T - 25)$

where S is the salinity of the aqueous phase (wt% of NaCl), EACN or the equivalent alkane carbon number is a measure of the hydrophobicity of the oil phase, T is the temperature in $^{\circ}C$, σ and β are the characteristic parameters of surfactant, $f(\mathrm{A})$ and $\varphi(\mathrm{A})$ are alcohol co-surfactant parameters, and constants K, b, a_T, c_T are positive constants depending on the system. The sign beside each parameter in the equations above represents the direction of the change in HLD as the parameter increases. As mentioned before, HLD can be either positive, negative or zero. As the phase inversion point of HLD = 0 is approached from either the positive or negative side, the interfacial tension decreases in magnitude precipitously, and attains ultralow values (~ 1 μN/m) [22,59]. Near HLD = 0, the oil-water mixture can be emulsified with minimal input of energy due to the ultralow interfacial tensions. The emulsion, however, can also destabilize rapidly when shearing is stopped, provided there exists an adequate collision rate between the droplets. This is, again, on account of the low interfacial tension that promotes higher bridge formation rates between two drops and shortens the time to coalescence. To make a stable emulsion, the surfactant for a given oil and aqueous phase combination must be selected such that the HLD is small in magnitude, to ensure low interfacial tensions that allow drop breakup, but not too close to HLD = 0 where coalescence rates are high [59]. A recent advancement [57,58] to the HLD framework is the net average curvature (NAC) model. The NAC model considers two curvatures: the difference between the two principal curvatures of the interface, termed as net curvature, and the mean of the two principal curvatures, termed as the average curvature. The net surfactant membrane curvature is modelled to be proportional to the HLD, as it is a measure of the free energy cost required to change the net curvature of the interface from a given value to a net zero value corresponding to a bicontinuous emulsion phase. The inverse of the proportionality constant is an empirically determined length scale, which can be related to the length of the extended tail of the surfactant, and is a measure of its solubilization capability. The inverse of the average curvature defines another length scale, which characterizes the ability of the surfactant to solubilize oil and water. Knowledge of the net and average curvatures allows the prediction of the interfacial tension, viscosity, phase transitions, phase volumes and solubilization capacity of the emulsion for ionic surfactants [61], non-ionic surfactants [56] and their mixtures [57].

Once the emulsifier is identified, it is also important to consider how much surfactant needs to be added to obtain an emulsion. Adsorbed emulsifier molecules at the interface occupy a finite area per molecule, so there is an upper limit on the interfacial concentration of the species for monolayers [42]. At low bulk concentrations, most of the emulsifier molecules are isolated monomers in the solution, and the interfacial concentration of the surfactants is below the maximum value. As the bulk concentration increases, the interfacial concentration increases, but simultaneously, the likelihood of aggregation of the surfactants in bulk also increases due to the possibility of the aggregate having a lower enthalpy than the individual molecules. The concentration at which bulk surfactant molecules contribute to aggregates rather than adsorb at

the interface is called the *critical micelle concentration* (CMC). Beyond the CMC, increasing the concentration of the emulsifier does not reduce the interfacial tension any further, and the interfacial concentration of the surfactant layer at the interface reaches the maximum value [62]. Typically, concentrations greater than the CMC are chosen to formulate stable emulsions. Stable dispersed droplets are generally formed only if there is a sufficient amount of emulsifier available to adsorb on to all the available droplet surfaces (Fig. 1a). However, concentrations much greater than the CMC could change the rheology of the aqueous phase to promote foaming (due to the trapped gas or liquid), which increases the bulk viscosity and can even lead to rigidification of the interface [51].

A third consideration while selecting emulsifiers is the time required for the surfactant molecules to cover the interfaces of the droplets. As illustrated in Fig. 1b, at concentrations close to and above CMC, when emulsifiers adsorb on to the droplet surface but do not yet fully cover it, the IFT is time-dependent and is known as the dynamic IFT. When the surface and bulk concentrations of the emulsifier reach equilibrium, the IFT reaches an equilibrium value. The time required to attain the equilibrium IFT determines how long the droplets produced in an emulsifier need to be placed in contact with the medium containing the emulsifier. The time scale depends on the amount of emulsifiers, the drop size, the mass transfer coefficients for surfactant exchange between the bulk and the interface, and the rates of their adsorptive and desorptive exchanges between the subsurface and the interface [63,64]. Thus, with the correct emulsifier for an oil-water system, the appropriate flow conditions to cause drop breakup, and adequate time afforded for the emulsifying

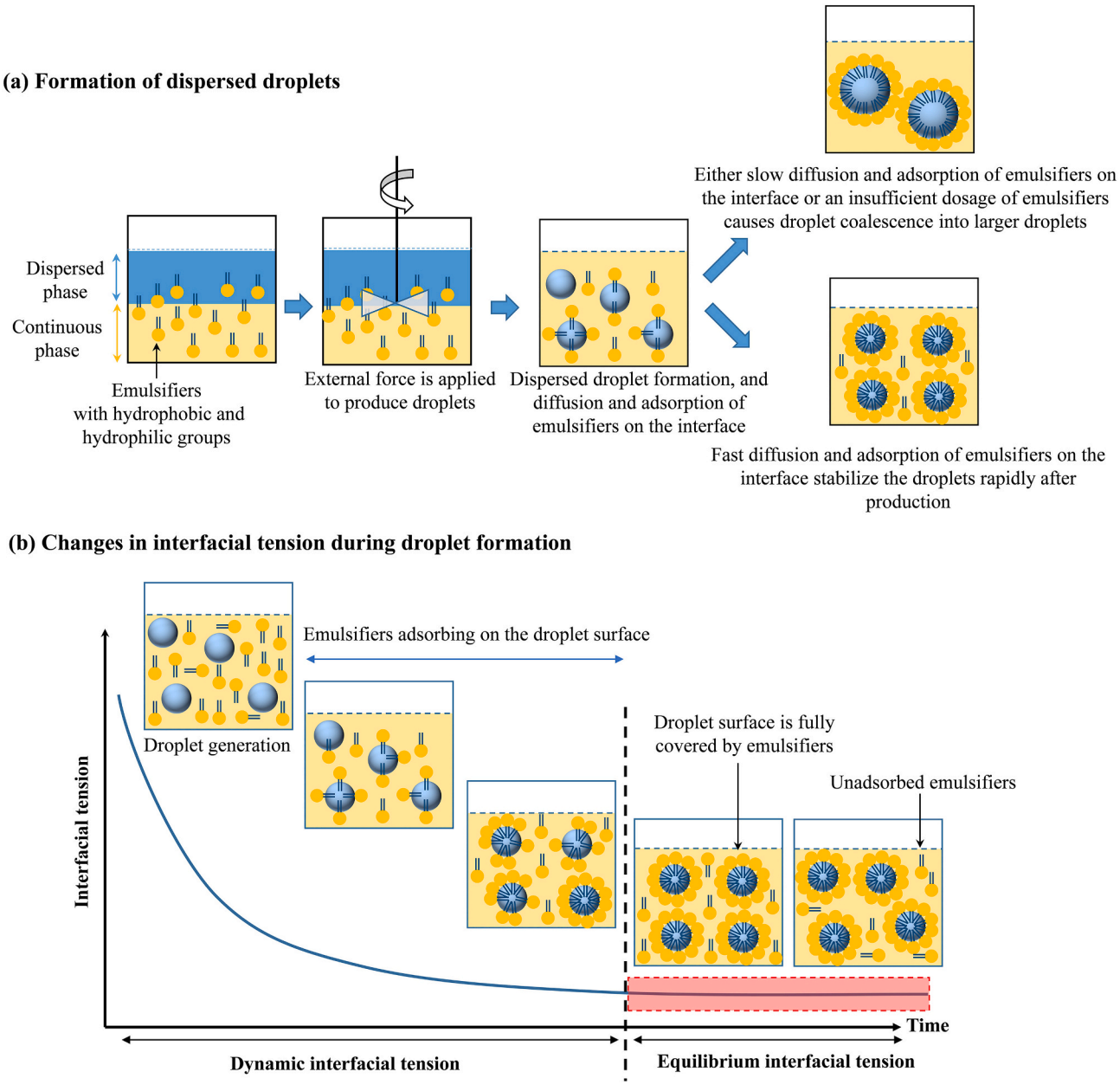

Fig. 1. (a): Formation of dispersed droplets in the presence of emulsifiers; depending on the amount of the emulsifiers and their rates of diffusion to and adsorption on the interface, newly generated dispersed droplets either are stabilized immediately after they are produced, or coalesce together. **(b)**: Changes of interfacial tension (IFT) during droplet formation due to adsorption of emulsifiers; reduction of IFT associated with adsorption of emulsifiers until an equilibrium IFT value is reached is characterized as dynamic IFT, while IFT value determined when emulsifiers cover the interface (corresponding to equilibrium) is known as equilibrium IFT. At equilibrium, unadsorbed emulsifiers exist as micelles in the continuous phase when the bulk concentration is above the critical micelle concentration (CMC).

surfactants to cover the interfaces of the drops, emulsifiers can significantly retard coalescence, resulting in a stable emulsion.

2.4. Destabilization processes

Stability of dispersed droplets from the generation point to the end-use determines the overall stability of emulsions during their shelf-life. Destabilization of dispersed droplets or emulsions is induced by a combination of several physicochemical processes: creaming and/or sedimentation, flocculation, coalescence, partial coalescence, Ostwald ripening, or even phase inversion. These destabilization processes are described in Fig. 2. At the stage of dispersed droplet formation, coalescence between droplets due to collisions is the main destabilization mechanism. In many cases, coalescence can be extremely rapid particularly during the initial period of emulsification, making the investigation of these phenomena very difficult. However, using suitable microfluidic devices with collision channels/chambers, instability of a single droplet during generation can be determined [11]. For determining long-term stability of emulsions, together with typical methods, reported in great detail by Mcclements (2007) [1], it is still possible to employ microfluidic devices, particularly the microcentrifuge, which allows the study of emulsion droplet coalescence under enhanced gravity [15]. In the following section, various types of microfluidic devices that can be used as an analytical tool for determination of IFT and stability of emulsions to coalescence are described.

3. Microfluidic devices for emulsion characterization

3.1. Types of microfluidic devices

Many microfluidic systems have been introduced for measurement of emulsion properties. These systems have specifically designed geometries to form dispersed droplets in the continuous phase, to measure the dynamic and equilibrium IFT, and to ascertain the stability of the droplets against coalescence. There are many reported configurations of such systems, and they can be classified into two main groups depending on the mechanisms to form dispersed droplets, namely shear-based systems, which break droplets during stretching, and geometry-induced capillary breakup systems, which break droplets during relaxation after deformation. In the shear-based systems, two fluids move inside individual channels and meet at a junction where dispersed droplets are detached and generated. The formation of dispersed droplets is a result of extensional stresses exerted by the continuous phase moving either in cross-flowing (e.g. T-junction and Y-junction) or co-flowing configuration with respect to the dispersed phase flow (Fig. 3a). On the other hand, in geometry-induced capillary breakup systems, also known as microchannel arrays, the dispersed phase is pressurized to travel through a shallow, confining microstructure and subsequently into a region where the geometrical confinement is relieved. Consequently, dispersed phase droplets are generated in the continuous phase by breakup during the shape relaxation process. Corresponding to the structure of microchannel arrays, there are three well-known geometry-induced capillary breakup systems (Fig. 3b): terrace based microchannel (1), straight-through microchannel (2), and edge-based droplet generation devices (3). In both shear-based and geometry-induced breakup systems, the size distribution of the droplets generated during emulsification is primarily determined by the microfluidic geometry and the dimensions of the pore, nozzle, or channel. Other important factors include flow rates of the phases involved in the emulsification process, the presence of emulsifiers and their concentrations, the IFT, the viscosities of the phases, emulsification temperature, and surface properties (e.g. wettability and roughness) of microfluidic systems. All these factors together control the formation and breakup of droplets during emulsification. For a microfluidic system with a defined geometry, the viscosities and the flow rates of the phases determine the force balance, the flow regime and the velocity profiles of the phases. The viscosities of the phases also affect the mass transfer and adsorption kinetics of the emulsifiers, which are typically pre-dissolved in the continuous phase prior to droplet formation. The emulsification temperature affects the viscosities of the phases and the IFT, and possibly the solubility of the emulsifiers. In addition, surface properties, particularly the wettability of materials used to produce microfluidic

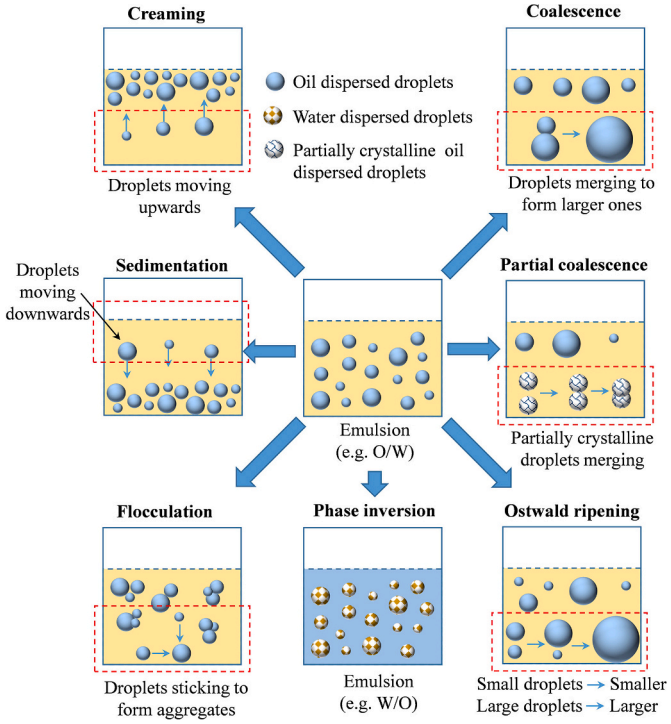

Fig. 2. A sketch describing possible instability processes of emulsions, dotted rectangles indicate the mechanisms of processes (Adapted with permission from McClements (2007) [1]).

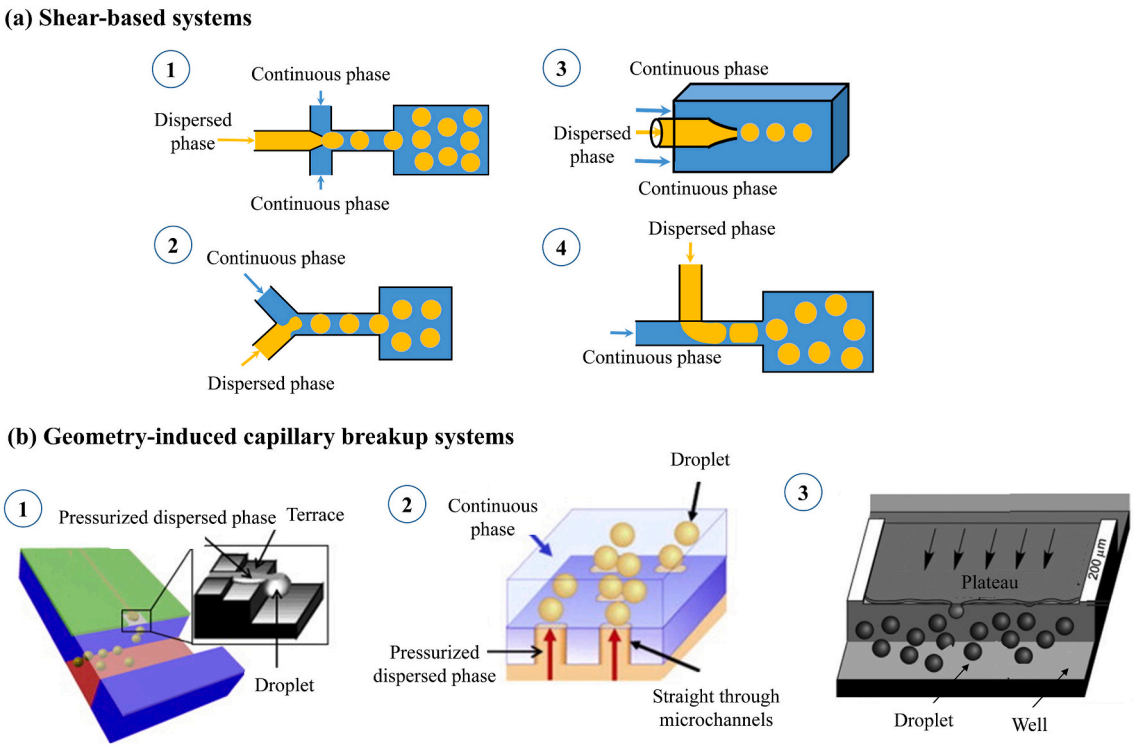

Fig. 3. Some configurations of microfluidic devices used for emulsion characterization. **(a)**: Shear-based systems (e.g. flow focusing (1), Y-junction (2), co-flowing (3) and T-junction (4)). **(b)**: Geometry-induced capillary breakup systems (e.g. terrace based microchannels (1), straight-through microchannel device (2), and edge-based droplet generation (3)). These sketches are not drawn to scale. Figure b(1–3) were adapted with permission from van Dijke et al. (2008) [67] and Sugiura et al. (2002) [68]; Kobayashi et al. (2008) [69]; and van Dijke et al. (2010) [70], respectively.

systems greatly influence the formation of droplets. The continuous phase should wet the surfaces of channels in microfluidic systems to enable the droplet formation and hence, the channel surface should be hydrophobic for W/O emulsification and hydrophilic for O/W emulsification. By controlling these factors, microfluidic systems have been successfully applied to study formation and breakup characteristics of droplets in simple emulsions, multiple emulsions, microspheres and microcapsules. These systems are described in greater detail elsewhere [7,16,65,66].

3.2. Materials for the fabrication of microfluidic devices

The materials used to construct microfluidic devices determine their functionalities. Depending on the purposes (e.g. research or commercial use) and application areas (e.g. bioengineering, chemistry, pharmacy, cosmetic or food), microfluidic device materials need to be carefully selected to achieve specific requirements. Other important aspects to be considered are the ease and cost of fabrication of microfluidic devices. Since the inception of fabrication methods for microfluidic geometries (e.g. photolithography in 1950s, and soft lithography in 1980s) [71,72], many types of materials have been investigated for the construction of microfluidic devices, offering a broad range of physicochemical surface properties and applications, namely inorganic materials (e.g. silicon, glass and ceramic), polymers (e.g. elastomers, thermosets and thermoplastics), hydrogels, biodegradable materials (e.g. polycaprolactone and polyglycolic acid), paper and fabric. The main properties of these materials are well described by Ren et al. (2013) [73]. Extremely low cost materials such as silk yarns and cotton threads have been successfully applied in the manufacture of microfluidic chips for electroanalytical and immunoassay applications. Along with low cost and high disposability, these materials enable the easy manufacture of microfluidic chips due to the simple assembly process [74,75]. In addition, several comprehensive reports have provided overviews of these materials for microfluidic applications, including properties, techniques for the microfabrication and surface modification, and their applications in various fields [73,76–79]. Therefore, only materials relating to emulsion investigations are described in this section.

Among these materials, glasses and polymers such as polydimethylsiloxane (PDMS), polymethylmethacrylate (PMMA), polycarbonate (PC) and polystyrene (PS), are the most widely used substrates for the fabrication of microfluidic devices in research laboratories. A large proportion of research papers published on microfluidic devices employs these materials [76]. A significant advantage of glass and polymers over other materials is optical transparency, which allows direct imaging of the movement of dispersed droplets inside the microchannels. This is an essential requirement in the characterization of emulsions, as high speed cameras capable of capturing images with exposures of less than a millisecond can be employed to visualize the events of moving dispersed droplets, from which the interfacial properties of droplets can be determined. Other advantages of using glasses and polymers are the ease and relatively low cost of fabrication, and biological compatibility [73,77,79]. In the formation of emulsions using microfluidic devices, the type of dispersed droplets formed is dictated, in part, by the intrinsic wettability of the liquid contacting microchannel walls. For example, O/W emulsion droplets are difficult to generate in a controllable manner in hydrophobic microchannels because the oil occupies the wall surface more readily than water [80]. As a result, glass and oxidised silicon with intrinsically hydrophilic surfaces are preferred for making O/W emulsions while polymers with highly hydrophobic surfaces are best for preparing W/O emulsions. However, the hydrophobicity or hydrophilicity of the microchannel surface can be modified to achieve the desired surface wettability. The common surface modification techniques include plasma treatment, UV irradiation, chemical vapour deposition, silanization, hydrosilylation, bulk modification with nanomaterials, sol-gel chemistry, dynamic coating with surfactants, and graft polymer coating. These techniques can result in deposition of new

and/or conversion of native surface layers, which are different in thickness, uniformity, roughness and topography. Thus, a suitable surface modification technique is selected depending on materials of microfluidic systems, experimental conditions and desirable surface properties. Details of these techniques have been described well elsewhere [81–85]. Table 1 summarizes several techniques for modifying the surface properties of microfluidic materials (e.g. glass and polymers).

4. Emulsion characterization using microfluidic devices

4.1. Determination of interfacial tension

IFT is an important physical property determining the sizes of the droplets, and the structure, the dynamics and the stability of emulsions. Different tensiometric techniques are commercially available for the accurate and reliable measurements of both equilibrium and dynamic IFT of the interface between two immiscible fluids, and provide insights into interfacial processes, especially the adsorption behavior of emulsifiers. These techniques include Wilhelmy plate, Du Noüy ring, pendant drop, sessile drop, maximum bubble pressure, oscillating jet, growing drop, and pulsating bubble methods. The details of the theoretical background and experimental techniques of these methods have been reviewed by Dukhin et al. (1995) [105] and Drelich et al. (2002) [106]. There are several limitations associated with these methods, such as the requirement of relatively large amounts of samples and very long monolayer equilibration times. Recently, microfluidic techniques have emerged as alternative methods to quantify the IFT of emulsions with many advantages over traditional tensiometric methods, including the compact size, the portability, the use of very small sample volumes (few mL), and the high repeatability and sensitivity. Importantly, they allow the monitoring of the IFT of emulsions at very short time scales after interface creation, which is difficult to achieve when using many aforementioned traditional methods, especially when emulsions are stabilized by highly active surfactants [107]. However, in order to determine the IFT using the microfluidic devices, theoretical models describing the relationship between IFT and droplet properties are required, and physiochemical properties of both fluids (e.g. viscosities and densities) at the measuring conditions need to be precisely measured. A summary of studies that use microfluidic devices to probe the IFT is illustrated in Table 2, which indicates that microfluidic tensiometers can be classified into two categories: fluid-fluid interface-based systems (Fig. 4) and droplet-based systems (Fig. 5). In the first category, two fluids are brought into contact with each other to create an interface at which the IFT is determined while in the second category, droplets are generated and the IFT of droplet-medium interface is measured. The accuracy, reliability, and effectiveness of microfluidic systems are evaluated by comparing the IFT results determined by the microfluidic devices with existing reference data and/or those measured by commercial tensiometers.

Table 1
A summary of studies using common techniques to modify the surface of microfluidic systems.

Techniques	Materials	Water contact angle (°)	Modified surface stability	References
Ultraviolet graft polymerization*	PDMS	45	Stable (> 30 h)	[86]
Oxygen plasma treatment	PMMA	70	No change up to 2 h	[87]
Gas-phase reaction with HFTTCS		> 145	Not determined	
Oxygen plasma treatment + gas-phase reaction with HFTTCS		> 145	Not determined	
Oxygen plasma treatment + solution-phase reaction with HFTTCS dissolved in FC-3283		125	Not determined	
Glass coating via sol-gel chemistry	PDMS	105	Not determined	[88]
Glass coating via sol-gel chemistry + PAA grafted surface		22		
Light-induced polymerization	PNIPAAm-modified glass	30	Not determined	[89]
UV/ozone – 120 min	PDMS	46	Stable (> 3 months)	[90]
Air plasma treatment	PDMS	38.23	Changes with time	[91]
Extraction with triethylamine, ethylacetate and acetone		57.6	Stable	
HEMA grafting		41.0	Stable	
PEG UV-grafting		69.9	Stable	
Oxygen plasma treatment and/or heating 200 °C for 3 h	PDMS-glass hybrid	109	Not determined	[92]
Silane-based “click” chemistry	Glass	33–59	Not determined	[93]
Oxygen plasma treatment	PMMA	≤ 5	Stable (20 days)	[94]
	PEEK		Stable (60 days)	
C4F8 plasma deposition + Oxygen plasma treatment	PMMA, PEEK	153	Stable (months)	
Oxygen plasma treatment	PDMS	8	Stable (after 5 days 85% recovery)	[95]
Oxygen plasma treatment + b-PEI		32	Stable (5 days)	
Dynamic coating (23–70 °C) with dodecylamine (5% *w*/w) in methanol, ethanol and isopropanol	Polycarbonate	70–135	Stable (4 days)	[96]
Ultraviolet light 172 nm in wavelength under pressures of 10, 10^3, 10^5 Pa for 600 s	Polystyrene	0–8	Stable (only 10 Pa for 30 days)	[97]
Chemical vapour deposition with poly(PFDA-*co*-EGDA)	PDMS	82.7–120.7	Not determined	[98]
Helium plasma polymerization of acrylic acid	PDMS	9.6	Stable (4 weeks)	[99]
Entrapment functionalization of acetone, n-pentane and FOTS	Polycarbonate	115	Stable (2 days)	[100]
Deposition of silica nanoparticle layer + silanization with n-dodecyltrichlorosilane	PMMA, PET and PVC	< 5	Stable (6 moths)	[101]
Coating with thin film of gallium by evaporation	PDMS, Si, SiO_2, SU-8, Glass and parylene-C coated PDMS	164–165	Not determined	[102]
Deposition of polyvinyl alcohol (87% hydrolysis) + oxygen plasma treatment (100 W for 1 min)	PDMS	~ 21	Stable (30 days)	[103]
Dynamic coating process with a nano-colloidal TiO_2 sol + UV irradiation	COC	10	Stable (10 months)	[104]

* Acrylic acid, acrylamide, dimethylacrylamide, 2-hydroxylethyl acrylate, and poly(ethylene glycol)-monomethoxyl acrylate; **PDMS**: Poly(dimethylsiloxane); **PMMA**: Poly(methyl methacrylate); **HFTTCS**: Heptadecafluoro-1,1,2,2-tetrahydrodecyl trichlorosilane; **FC-3283**: Perfluorotripropylamine; **PAA**: Polyacrylic acid; **PNIPAAm**: Poly(n-isopropylacrylamide); **HEMA**: 2-hydroxyethyl methacrylate; **PEG**: polyethylene glycol; **PEEK**: poly(ether ether ketone); **C4F8**: Octafluorocyclobutane; **b-PEI**: branchedpolyethylenimine; **PFDA**: 1H,1H,2H,2H-perfluorodecyl acrylate; **EGDA**: ethylene glycol diacrylate; **FOTS**: 1H,1H,2H,2H-perfluorooctyl trichlorosilane; **PET**: Polyethylene terephthalate, **PVC**: Polyvinyl chloride; **COC**: cyclic olefin copolymer.

4.1.1. Interface-based systems

The micropipette technique is probably the first reported microfluidic strategy for the determination of the equilibrium and dynamic IFT of micro-scale interfaces, of two immiscible fluids (e.g. water-decane, water-hexadecane and water-chloroform), stabilized by an emulsifier (e.g. sodium dodecyl sulphate) [108]. In this technique (Fig. 4a), a fresh, curved interface between two immiscible fluids (with a curvature radius of 1–100 μm) is generated in a tapered micropipette, then a second pipette with a smaller internal diameter than that of the measuring pipette is used to deliver emulsifier solution directly to the generated interface. The IFT is quantified from the changes in the interfacial curvature at given applied pressures via the Young-Laplace equation. Mimicking this technique, Gu et al. (2011) [109] introduced a tapered microchannel tensiometer (Fig. 4b), but accounted for the contact angles in the calculation of interface curvature radius in both horizontal and vertical directions. The equilibrium IFT values of the interfaces of mineral oils and water in the presence of an emulsifier (e.g. Span 80) determined by this approach were highly comparable to macroscopic measurements, and the technique could be applied for measuring IFT that changes over time (in a range of 3–38 mN/m). However, this system was limited to interfaces without surfactant or with small amounts of surfactants due to contact angle hysteresis and pinning. Swelling of the material used to design the microchannel (e.g. PDMS), which occurs in various solvents and changes the channel geometry in an uncontrolled manner, is another limitation of this system. Thus, chemically inert materials must be chosen to design the microchannel to expand the versatility of the system. In addition, both micropipette and microchannel systems require highly precise pressure transducers to obtain reliable results. Zhou et al. (2013) [110] developed a microfluidic device consisting of a pair of Laplace pressure sensors (Fig. 4c), allowing measurement of the pressure drop across the microchannel. IFT was inferred from the pressure drop and the interfacial curvatures in the tapered channel. The use of a pair of Laplace sensors also offers other benefits through the elimination of calculation of interfacial curvature in the vertical direction, and possible effects of the flow and/or geometry changes in the microchannel. Thus, this system overcomes the limitation of micropipette and microchannel systems as it no longer requires highly precise pressure sensors. This setup allows determination of the equilibrium IFT of water with mineral oil (48.3 mN/m), silicone oil (25.2 mN/m), hexadecane (43.5 mN/m), and soybean oil (24.8 mN/m), with accuracies comparable to a commercial tensiometer. In addition, the working principle of this microfluidic device is not dependent on the properties of the fluids, thus its applicability for IFT measurement is very versatile, including immiscible liquid-liquid, liquid-gas systems, or more complex mixtures with surfactants (e.g. Span 80 in mineral oil/water system). As compared to micropipette and microchannel systems [108,109], this microfluidic device is more robust and easier to implement for IFT measurement.

Unlike the above microfluidic systems [108–110] which are dedicated to typically high IFT values (e.g. > 1 mN/m), Tsai et al. (2013) [111] reported a microfluidic tensiometer for determining ultralow IFT values of 10^{-3}–10^{-2} mN/m for the interfaces between oil phase (Span 80 and dodecane mixture) and aqueous phase (sodium dodecyl sulphate (SDS), glycerol and water mixture). As shown in Fig. 4d, the system comprises a co-flow junction where the aqueous solution flows through the inlets to the centre and encounters paramagnetic beads (which are supplied through another central inlet) while the oil phase is supplied through a side inlet to form a co-flow with the aqueous fluid and the beads. By applying external magnetic fields to paramagnetic spheres, a critical dimensionless distance between the paramagnetic beads' centre and the interface was observed, from which magnetic forces acting on the beads were calculated. The IFT was then estimated from a force balance between magnetic and interfacial forces on the beads. Therefore, the IFT range measured by this microfluidic tensiometer is limited by the magnetic force that can be exerted on the sphere.

4.1.2. Droplet-based systems

Hudson et al. (2005) [112] and Cabral and Hudson (2006) [113] were the pioneers of the droplet-based microfluidic tensiometer for measuring the IFT of droplets dispersed in continuous phase. The system (as shown in Fig. 5a) consists of a T-junction where dispersed droplets are generated. Fluid 1 (a and b) is injected as droplets into immiscible fluid 2. Then, these droplets are fed via 3a and 3b channels into a flow constriction downstream channel 4 where the droplet deformation is observed. The channels 3a and 3b can be used to accelerate the newly formed droplets and maintain the original droplet velocity. Based on Taylor's theory [40] for drop deformation in extensional flow fields, the equilibrium IFT of water, ethylene glycol, or glycerol droplets in silicone and mineral oils, even of multicomponent droplets (e.g. water/ethylene glycol droplets in silicone oils) with the values from 2.5 to 60 mN/m could be deduced, and the results were in agreement with existing published data and those from conventional measurements [112–114]. However, the precision and accuracy of this system for IFT measurement are greatly affected by the focusing and threshold level in the image analysis, the size of channels, and the flow rate of droplets and surrounding fluid. For image analysis to determine the droplet shape, the light intensity and focusing adjustment, and the setting of a binary threshold value are manually executed. Therefore, poor focusing can lead to an offset in the measured IFT values of up to 20% while inappropriate setting of the threshold level (with good focusing) results in an error of about 5%. When the relative viscosity between the droplets and continuous fluid (λ) is less than 0.03, the measured IFT values are almost unchanged at the ratio of droplet diameter and the smallest channel height (d/h) of 0.2–0.7. However, the measured IFT is greatly affected as $d/h > 0.8$ and $\lambda > 0.03$ at which the droplets experience a significant drag force. In the presence of highly active surfactants in the measuring system, the flow rate of droplets and surrounding fluid greatly affects the measured IFT. Since the initial report of Hudson et al. (2005) [112], various configurations of T-junction microfluidic tensiometers have been developed for the determination of IFT as a function of emulsifier concentration and adsorption time. Nguyen et al. (2007) [115] reported a T-junction microfluidic tensiometer to measure equilibrium IFT values of water-silicone oil interface stabilized by cetyl trimethyl ammonium bromide (38.6–75.5 mN/m) based on the formation frequency of dispersed droplets (Fig. 5b). However, this system determined IFT values accurately only for surfactant concentrations up to CMC, as the relation of the formation frequency of dispersed droplets and the measured IFT was linear. Beyond the CMC, the formation frequency of dispersed droplets changed sharply and correlated poorly with IFT. Wang et al. (2009) [116] presented another configuration of T-junction microfluidic device (Fig. 5c), allowing the determination of the dynamic IFT at the rupturing moment (5–50 mN/m) of water-hexane stabilized by Tween 20 at concentrations much higher than its CMC (0.03 mmol/L), based on the sizes of dispersed droplets. From this system, it was reported that the average diameter of formed droplets changed with varying Tween 20 concentrations of up to 10 mmol/L, but showed almost no change at higher concentrations due to the saturation of the interface by the adsorbed surfactant. However, by using a pressure-drop based T-junction microfluidic device (Fig. 5d), Wang et al. (2015) [117] revealed that, at the point of rupture of water-octane interface stabilized by SDS and Tween 20, while the surfactants had almost completely adsorbed to the interface and the droplet size-based microfluidic device [116] could not measure any IFT difference at this breakup moment, there still was an alteration of IFT as the droplet started to leave the wall of the T-junction side channel. This indicates an advantage of the pressure-drop based T-junction microfluidic device over the droplet size-based counterpart.

Other microfluidic systems were also investigated for IFT measurements, such as an array of microstructures, a series of expansions and contractions, coaxial flows, and Y-junction devices, with highly accurate results. For devices with microstructure arrays (Fig. 5e), the dispersed phase is pumped into an array of microchannels and droplets are

Table 2
A summary of studies using microfluidic devices to probe interfacial tension (IFT).

Emulsions		Microfluidic device	IFT type	Theory for IFT calculation	References
Dispersed phase	**Continuous phase**				
Water Sodium dodecyl sulphate (SDS)*	Decane, hexadecane and chloroform	Micropipette (Fig. 4a)	Equilibrium and dynamic	Radius of curvature of interface vs. externally controlled pressure drops based on Young-Laplace equation	[108]
Mineral oil Span 80 (0.5–1%)*	Water Triton X-100 (0.5%)*	Tapered microchannel (Fig. 4b)			[109]
Mineral oil, silicone oil, hexadecane and soybean oil Span 80 (~ 0.1 mM)*	Water	A pair of tapered microchannels (Fig. 4c)	Equilibrium and dynamic	Pressure drop across a microchannel vs. interfacial curvatures	[110]
Dodecane Span 80 (10%)	Water Glycerol (25%) SDS (4–20 mM)*	Microfluidic ultralow interfacial tensiometer with magnetic particles (Fig. 4d)	Ultralow	Deformation and retraction of droplets under converging or diverging flow based on Taylor's theory	[111]
Silicone oil, glycerol and water	Silicone oils and glycerol	T-junction connected to microchannel with/without constrictions (Figs. 5a-d)	Equilibrium		[112]
Ethylene glycol (EG) and water-EG mixtures	Silicone				[113]
Mineral oil# n-butanol (0.2–5%)*	Water# n-butanol (0.2–5%)*				[114]
Water Cetyl trimethyl ammonium bromide (0–10^{-2} M)*	Silicone oil		Equilibrium	Droplet formation frequency	[115]
Hexane	Water Tween 20 (0.8–20 mmol/L)*		Dynamic	Droplet size	[116]
n-octane	Water SDS (0.28%)* Tween 20 (0.07%)*			Pressure drop during droplet formation	[117]
Water and barium chloride solution	n-butyl alcohol, n-octyl alcohol, sulfuric acid & n-butyl alcohol solution, and silicon oils	A pore array micro-structured device (Fig. 5e)	Equilibrium	Flow resistance vs. the capillary pressure	[118]
Water-ethanol	Fluorinated oil Perfluorinated molecules (1.3–5.2 mol/m^3)*	A series of expansions (Fig. 5f)	Dynamic	Deformation of droplets vs. hydrodynamic forcing based on Taylor's theory	[119]
Butanol, hexane and octanol Span 80 (2%)*	Water Tween 20 (2%)*	Coaxial microfluidic device (Fig. 5g)	Equilibrium	Viscous force vs. interfacial tension force	[120]
Hexadecane	Water, ethanol solution, glycerol solution, and sucrose solution SDS (0.01–1%)*	Y-junction (Fig. 5h)	Equilibrium	Droplet size	[121]
Hexadecane	Water Tween 20 (2%)* Bovine serum albumin (0.25–1%)* Whey proteins (0.25–1%)		Equilibrium		[122]
Hexadecane	Water-ethanol solution SDS (0.03–3%)* Synperonic PEF108 (0.025–5%)*		Equilibrium and dynamic		[123]
Water Tween 20 (0.02–2%)*	Hexadecane Span 80 (0.3 and 3%)*	Glass aspiration capillary (Fig. 5i)	Equilibrium	Droplet radius vs. applied aspiration pressures based on Young-Laplace equation	[124]
Water and glycerol	Mineral and silicone oils	Temperature controlled tensiometer (Fig. 5j)	Temperature dependent	Deformation of droplets based on Taylor's theory	[126]
Water Polyoxyethylene-20 hexadecyl ether (10^{-7}–10^{-2} M)*	Soybean oil	Silica circular cross section microcapillary (Fig. 5k)	In situ		[125]
Water and glycerol	Mineral oil	Hele-Shaw microfluidic extensional flow device (Fig. 5l)	Equilibrium	Small deformation theory for pancake shaped droplets	[127]
Water	Bitumen solutions		Dynamic		
Glycerol solutions	Light and heavy mineral oils Span 80 (0.05% *v*/v)*	T-junction and four-channel microfluidic hydrodynamic trap	Dynamic	Droplet shape relaxation in confined regime	[128]
50% (w/w) aqueous glycerol	Oleic acid Span 80 (1% w/w)*	A flow-focusing and a cross junction region	Dynamic	Droplet deformation in confined or unconfined conditions using 2D Darcy approximation model and quasi-static 3D small deformation model	[129]
Synthetic sea water Simulated bilge detergent mix (25–100 ppm)* Alcohol ethoxy sulfate (10–100 ppm)*	Mixture of diesel fuel and lubrication oil	T-junction and a series of contraction chambers	Dynamic	Deformation of droplets based on Taylor's theory	[130]
Mixture of diesel fuel and lubrication oil	Synthetic sea water Simulated bilge detergent mix (25–100 ppm)* Alcohol ethoxy sulfate (10–100 ppm)*				

* Emulsifiers/surfactants
\# Emulsifiers can be in either dispersed or continuous phases.

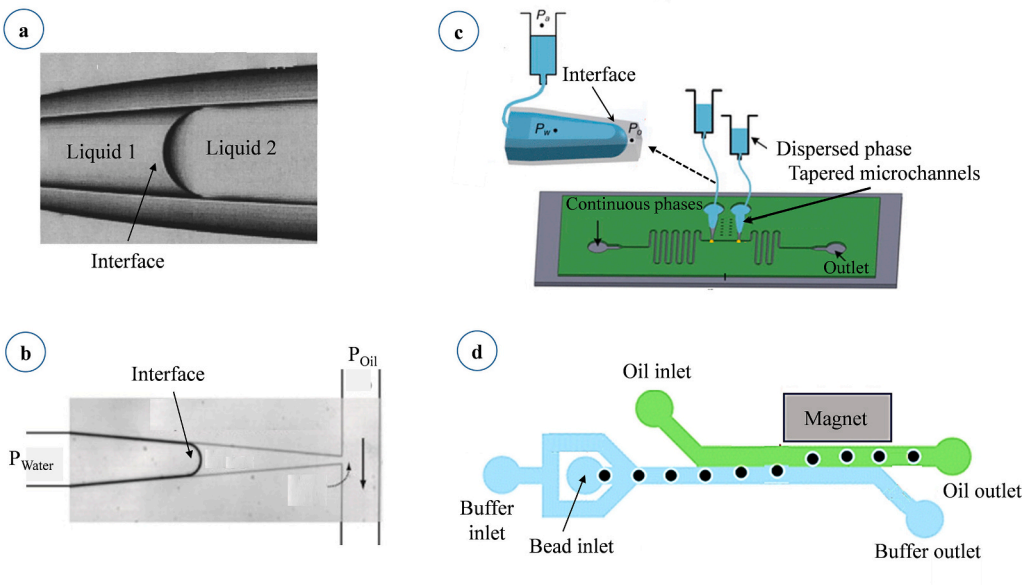

Fig. 4. Sketches of some microfluidic fluid interface-based devices to probe interfacial tension. **(a)**: Micropipette (Adapted with permission from Lee et al. (2001) [108]). **(b)**: Tapered microchannel tensiometer (Adapted with permission from Gu et al. (2011) [109]). **(c)**: A pair of tapered microchannels together with the interfaces produced in a tapered microchannel (Adapted with permission from Zhou et al. (2013) [110]). **(d)**: Microfluidic tensiometer with a co-flow geometry in which the aqueous and oil phases flow through the buffer and oil inlets, respectively; beads are supplied through another inlet, and permanent magnet draws paramagnetic beads passing through the interface (Adapted with permission from Tsai et al. (2013) [111]). These sketches are not drawn to scale.

generated by the shearing force of the cross-flowing continuous phase. By analyzing the competition between the flow resistance and the capillary pressure in the geometry, equilibrium IFT values (1–50 mN/m) of droplets (e.g. water or barium chloride/water) dispersed in either alcohols, sulfuric acid/alcohol or silicone oil (polydimethylsiloxane) were determined [118]. The accuracy and precision of the measurements are greatly dependent on the viscosity and the flow rate of the dispersed phase, and the active pore percentage. For a system with a chemical reaction - barium chloride/water in sulfuric acid/alcohol, the measured IFT values were smaller by 2% than those determined by the pendant drop method due to higher mass transfer rates in the microstructure array. This system is more practical for the measurement of the equilibrium IFT between immiscible fluids as only active pore number is required, and it can be counted by observation without quantitative determination. In the device with a series of expansions and contractions (Fig. 5f), the droplets (e.g. water-ethanol mixture in fluorinated oil) after being generated in a flow focusing junction were forced to pass through a series of expansions, which causes the droplet deformation. The dynamic IFT was inferred from the deformation of the droplets in each expansion-contraction section [119]. This microfluidic device can measure the IFT of droplets with very small droplet deformation, without relying on the assumption of specific droplet shapes during deformation. However, the microfabrication of the device is quite complicated. For coaxial devices, as shown in Fig. 5g, dispersed droplets (e.g. butanol, hexane or octanol) are formed at outlet end of a microneedle, and then co-flow with continuous phase (e.g. water) into a larger channel. The IFT with and without emulsifiers (Tween 20 and Span 80) in a range of 1 to 10 mN/m could be determined from a force balance between the viscous drag force and the IFT force acting on the droplet [120]. The accuracy and precision of the measurement are dependent on the determination of the droplet size, the continuous phase viscosity, and the individual phase velocities. In this system, dispersed droplets are formed inside continuous phases, mitigating the disrupting effect of the wetting properties of microchannels on droplet formation. For Y-junction devices (Fig. 5h), dispersed and continuous phases flow in individual channels and meet at a Y-junction where droplets are generated. In such systems, droplet formation is determined by a balance between the shearing forces exerted by the continuous phase and the IFT forces keeping the generated droplets attached to dispersed phase, which affects droplet size. Both increasing shearing forces and lowering IFT forces facilitate droplet detachment and lead to smaller droplet size. Thus, the IFT at the moment of droplet formation can be calculated from droplet size. Unlike other microfluidic tensiometric methods [116,117,119] which have the capability of measuring IFT in the range of milliseconds to seconds, this Y-junction device is able to measure IFT changes within droplet formation times of 0.4–9.4 milliseconds. This technique was successfully applied to measure IFT of hexadecane droplets dispersed in either water, ethanol, glycerol, or sucrose solutions with SDS as emulsifier (15–46 mN/m) [121–123]; water-ethanol solution in the presence of SDS and synperonic PEF108 (10–41 mN/m) [127]; or water with Tween 20, bovine serum albumin and whey proteins (10–25 mN/m) [128]. Recently, Honaker et al. (2018) [124] reported a new and rapid microfluidic strategy for measuring IFT between two fluids without requiring their physical parameters. This method is the microfluidic version of the larger scale, micropipette aspiration technique for measuring the IFT of emulsion systems [131], which was initially developed to quantify the cortical tension of living cells or lipid membranes [108,132,133]. A diagram of such a device is illustrated in Fig. 5i. In this technique, dispersed droplets, which are initially generated in a glass injection capillary, are aspirated by applying pressure from the exit channel into either the tip of the droplet generation channel or the constriction at further down the collection capillary. By measuring the alterations of the droplet radius in the aspirated region in response to precise changes in suction pressure applied to the collection capillary (P to P + ΔP), the IFT is determined from Young-Laplace equation. This microfluidic system was successfully applied to measure IFT of water droplets in hexadecane, which were stabilized by Tween 20 at concentrations of 0.02–2.0% and Span 80 at concentrations of 0.03–0.3%. It could also possibly be applied to measure a wide range of IFTs from sub mN/m to several mN/m. However, the design of this system obviates the measurement of IFT immediately after droplet generation, and the accuracy of the IFT measurement is dependent on the resolution of the pressure pump. Also, the wetting of dispersed phase to the capillary walls could limit applicability of this system for measuring the IFT of different immiscible fluids.

Controlling localized temperature in the microfluidic devices is very

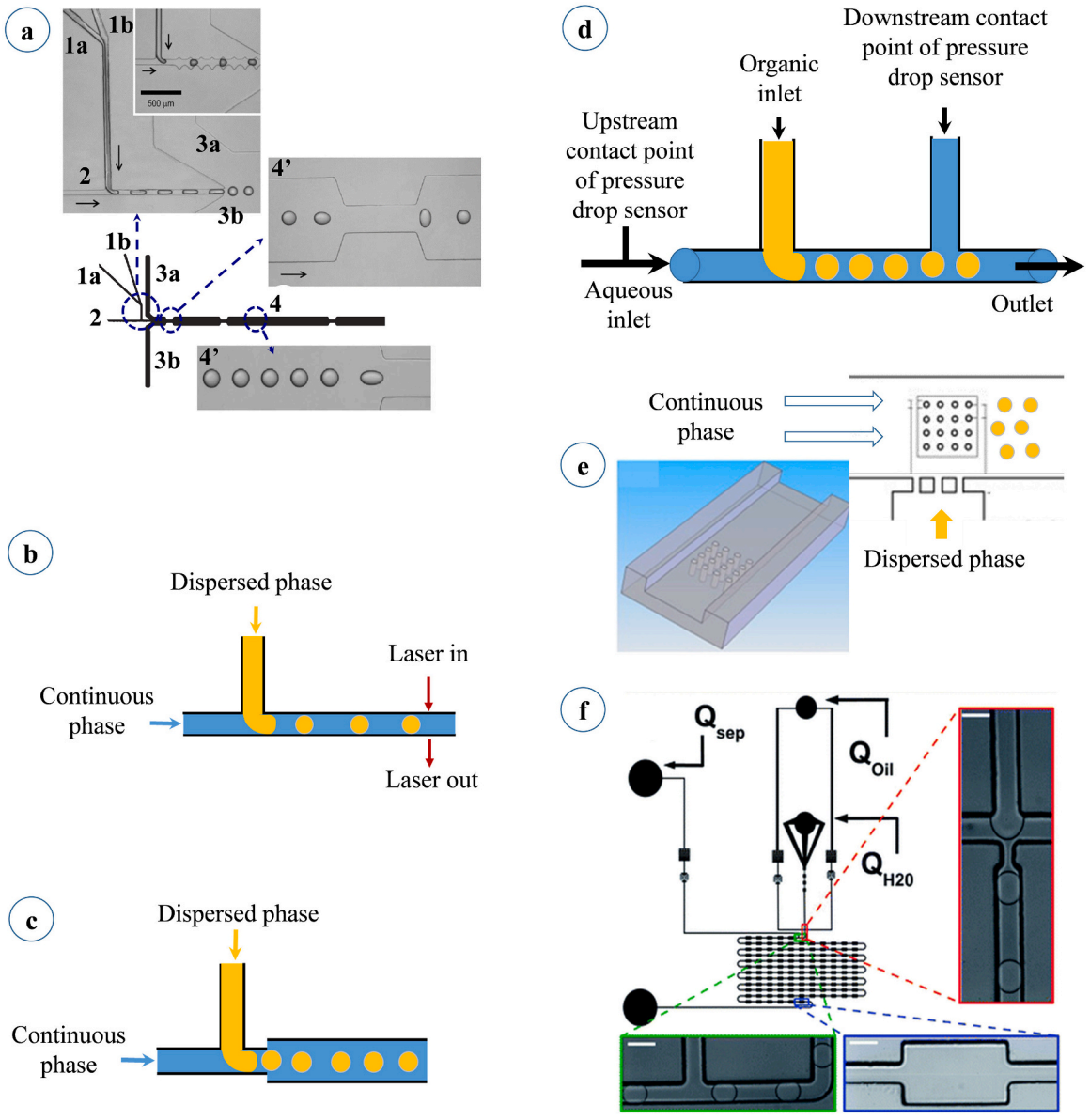

Fig. 5. Sketches of some microfluidic droplet-based devices to probe interfacial tension. **(a):** Droplet-based microfluidic tensiometer with T-junction (Adapted with permission from Hudson et al. (2005) [112]). Fluid 1 (a and b) is injected as droplets into immiscible fluid 2. Then, these droplets are fed via (3a) and (3b) inlets to channel (4) with a series of constrictions (4') to accelerate and stretch the droplets. **(b):** T-junction microfluidic geometry in which the droplets are formed in T-junction, and laser is employed to determine droplet formation frequency [115]. **(c)**: T-shaped microchannel in which the droplets are formed in T-junction, and alterations of droplet size during relaxation while flowing into a larger channel are detected (Adapted with permission from Wang et al. (2009) [116]). **(d):** T-junction microfluidic channel in which pressure drop during droplet formation is determined [117]. In this system, the microdroplets are formed in the first T-junction, while the second T-junction and the bifurcated feeding pipe are used to connect the pressure drop sensor. **(e):** Post array micro-structured device (Adapted with permission from Li et al. (2009) [118]). Two syringes are used to pump the continuous and dispersed phases to flow outside and inside the channel array, respectively. Droplets of the dispersed phase are formed by the cross-flow induced rupture in the main channel. **(f):** Microfluidic channel with a series of expansions (Adapted with permission Brosseau et al. (2014) [119]); Droplets are produced by focusing a stream of water in a stream of oil-surfactant solution, and the droplets then flow in a series of expanded sections where the droplet deformation profile is recorded and interfacial properties are analyzed. A series of expansions regularly distributed along a delay line is used to access the dynamics of the adsorption process during flow. **(g):** Coaxial microfluidic device (Adapted with permission from Xu et al. (2008) [120]). The dispersed droplets are formed in the coaxial geometry, and flow in the glass capillary. **(h):** Microfluidic Y-junction (Adapted with permission from Muijlwijk et al. (2016) [121]). In this system, the junction of the continuous and dispersed phase channels was a Y-shape with an angle of 97° between the continuous and dispersed phase channels. **(i)**: Flow-focusing devices used for measuring interfacial tension at the tip of the injection capillary (1) and at a constriction (2). In both systems, three experimental stages are illustrated, including droplet formation (1a' and 2a'); droplet being held stationary in the collection channel before aspiration into the injection channel (1b'), or just after the constriction (2b'), with pressure P applied from the collection tube exit; and aspiration of the droplet into the injection channel (1c' and 2c'), with a pressure $P + \Delta P$ applied from the exit of the collection channel (Adapted with permission from Honaker et al. (2018) [124]). **(j)**: Experimental apparatus of microcapillary (Adapted with permission from D'Apolito et al. (2018) [125]). The emulsion droplets are injected into the microcapillary from a glass syringe. **(k)**: Microfluidic tensiometer integrated with a temperature controller (Adapted with permission from Lee et al. (2017) [126]). This system consists of a droplet production region at a T-junction, a coflowing region, and a flow constriction region to deform the droplets, with precise on-chip temperature control. **(l):** The stagnation point device (Adapted with permission from Goel et al. (2019) [127]). The experiment to measure IFT using this system includes: a water drop entering into the diamond slot (1), the drop adopting the shape of an ellipse near the center of the device (2), and the drop leaving the channel (3). The sketch is not drawn to scale.

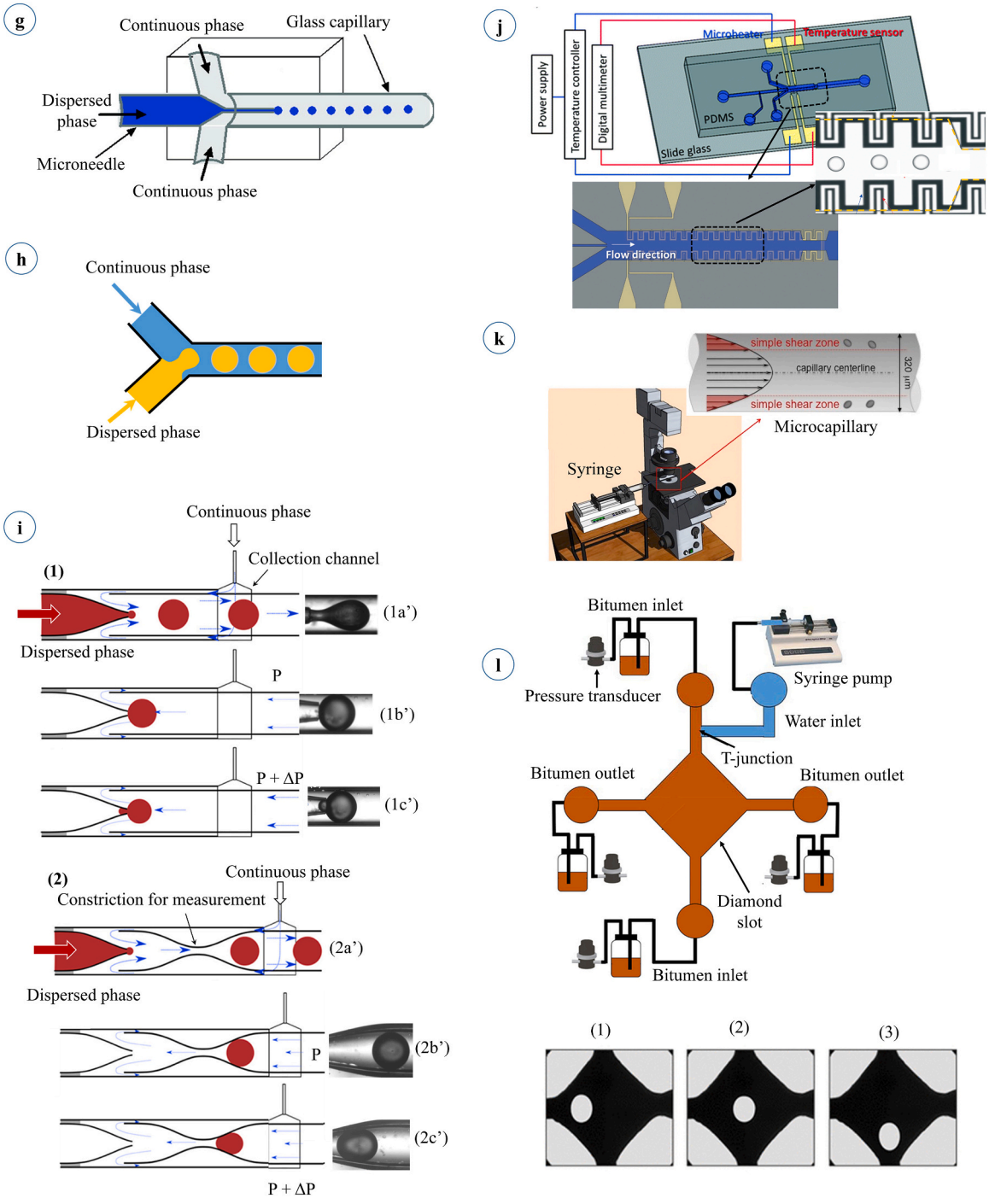

Fig. 5. (*continued*).

important to obtain precise results of IFT because temperature greatly affects not only the fluid viscosity, which is an indispensable parameter for IFT estimation via methods that involve flow, but also the adsorption kinetics of emulsifiers during droplet formation. However, most microfluidic studies including the aforementioned ones investigate the IFT of the fluid-fluid interface at room temperature without precise temperature control. Lee et al. (2017) [126] reported a microfluidic system (Fig. 5j) that allows accurate measurement of temperature-dependent IFT between two immiscible fluids. In this system, droplets generated in a T-junction are flowed downstream inside a microchannel, accelerated by two additional co-flowing streams, to a constriction region. The microfluidic platform is integrated with a localized temperature-controlled system that allows for precision control of the temperatures of the fluids within the device. Experimental results on the interfaces of droplets of water and glycerol in silicone and mineral oils indicated that the system had a capacity to measure IFT values (16.9–35.6 mN/m) from room temperature up to 70 °C, relying on Taylor's theory for droplet deformation in extensional flow fields.

Unlike previous droplet-based microfluidic approaches which require droplets to be generated within the devices and cannot accomplish the IFT measurement for droplet interfaces in emulsions as such, D'Apolito et al. (2018) [125] reported another microfluidic strategy that allows the determination of the IFT of droplets in pre-prepared emulsions. The system is quite simple (as shown in Fig. 5k), consisting of a

silica microcapillary with a circular cross section connected to a glass syringe and a syringe pump where the prepared emulsions are injected and flow rates of the injected emulsions in the microcapillary are controlled. Deformation of individual emulsion droplets in the region of steady state shear flow in the microcapillary, where the velocity profile is nearly linear, is analyzed basing on Taylor's theory, and from which IFT is obtained. This system allows the measurement of IFT of water droplets dispersed in soybean oil as a function of emulsifier concentration (7.4–27.6 mN/m). However, a disadvantage of this technique is that the dynamic IFT cannot be measured.

Another class of microfluidic devices that implements drop-based IFT measurement is that of stagnation point devices [128,129,134], and in particular, geometries that produce an extensional flow [128,135]. There are two versions of this device: the cross-slot [128,129,135], and the diamond shaped slot [127,136]. In this review, we will focus on the efforts from the Ramchandran lab in devising the microfluidic extensional flow device (MEFD), which employs the diamond-shaped slot, with one port at each node of the diamond, as shown in Fig. 5l. Two opposite ports bring fluid into the slot, and the other pair of opposite ports withdraws fluid from the slot. As a consequence, a stagnation point is developed within the slot, whose location depends on the incoming and outgoing flow rates through the ports. The slot is designed to be shallow, i.e. the width of the side of the diamond channel is much larger than its depth, usually by a factor of 10 or more. This limit allows the description of the flow field and the stagnation point inside the slot using an analytical solution [136] for arbitrary specification of the flow rates through the ports. This analytical solution is also the basis of a hydrodynamic trap, whereby any particle brought into the slot by the incoming flow through a port can be pushed towards the center of the slot and trapped there, theoretically indefinitely, by suitably placing the stagnation point around the particle within a feedback control loop. Drops generated upstream of the MEFD center at a T-junction can be brought to the center of the device and trapped there. Such a drop experiences a two-dimensional extensional flow field, and an analytical solution can be written to deduce the IFT from measurements of the drop deformation, the medium viscosity and the extensional rate. This approach allowed the measurement of ultralow IFT (in the order of tens of μN) [136]. The MEFD can also be used to measure IFT of the order of 10 mN/m, by continuously flowing a stream of drops through the MEFD, and deducing the IFT from the shape of the drop as it passes through the MEFD center [127,128,135]. By varying the flow rate, it is also possible to obtain the IFT as a function of the time elapsed from instant of drop generation at the T-junction. In the limit of kinetically controlled surfactant adsorption, this experiment provides the dynamic IFT. To examine whether surfactant adsorption is a kinetically-dominated or a diffusion dominated process, the time required to reach equilibrium IFT can be compared to the characteristic diffusion time, L^2/D, where L is the characteristic diffusion length in the bulk and is equal to the ratio of maximum interfacial concentration of the surfactant to the bulk surfactant concentration, while D is the diffusivity of the surfactant. If the time required to reach the equilibrium IFT is significantly longer than the characteristic diffusion time, then the surfactant adsorption process is kinetically limited.

By employing analytical solutions of the flow field and concentration boundary layers in the presence of a drop [127,136], it is also possible to study the rate of solubilization and the solubility of the drop fluid in the medium [137]. The production of satellite and sub-satellite droplets during drop breakup has been studied in detail in this geometry [48]. A key specialty of the approach is the use of Hele-Shaw drops, i.e. drops that have a diameter ($2R$) larger than the depth of the channel ($2b$), which are produced naturally in many microfluidic emulsion generation techniques (Fig. 3a; 1,2 and 4). When a Hele-Shaw drop is introduced into the diamond-shaped slot, it deforms into a pancake-like shape. While IFT measurements can be successfully performed with both small and moderate aspect ratio stagnation point devices [129], there are three important advantages of using pancake drops ($R > b$) as opposed to spherical drops ($R < b$). First, with spherical drops, one encounters the possibility of gravity taking the drop out of the microscope's focus. Also, settling changes the velocity field sampled by the drop, thus complicating the interpretation of drop deformation data and altering the mass transfer coefficient. On the other hand, Hele-Shaw drops span the entire thickness of the gap, and gravity plays a negligible role in the interaction of the drop with the extensional flow field. This is particularly advantageous in long time experiments where the drop needs to be monitored for several tens of minutes or even hours (e.g. in dissolution or precipitation studies). Second, the trapping and computer feedback control of a pancake drop is much easier than a spherical drop, particularly at higher strain rates, owing to the reduced mobility of the pancake drop relative to the spherical drop. Finally, when the suspending medium is nearly opaque, pancake drops are easier to locate and visualize than spherical drops. This feature becomes a significant advantage for media such as concentrated bitumen solutions, whose films are opaque beyond a few hundred microns of thickness [127]. A key challenge in these experiments, however, is the discovery of the correct surface treatment protocol for the microchannel to avoid the wetting of its surfaces by the drop fluid. As the drops in these experiments are in the Hele-Shaw or pancake configuration, it is essential to have a thin layer of suspending medium between the drop and the channel walls to allow the drop to move freely and prevent its contact with the top and bottom walls of the microchannel.

We end this section with a cautionary note; while microfluidic devices that measure IFT are aplenty, there are no existing microfluidic techniques that can measure other properties of fluid-fluid interfaces, such as the shear viscosity, the dilatational viscosity, and elastic properties. As mentioned in the section 2.1, the isotropic interfacial tension is the simplest model for describing stresses in interfaces, and while it works for many commonly encountered liquid-liquid interfaces, it is inadequate for complex interfaces. For example, for materials such as asphaltene-coated oil water interfaces [138] where interactions between interfacially adsorbed species upon interfacial deformation and shear are purported to lead to jamming or elastic effects, complex interfacial properties assume importance and can play a vital role in the phenomena of break-up and coalescence. Appropriate constitutive models then have to be adopted to describe the interfacial stress tensor. An avenue for future work is the combination and adaptation of existing microfluidic techniques to measure these additional properties.

4.2. Coalescence of droplets

The coalescence of droplets is an important destabilization process in emulsions, and involves the merging of two or more droplets to form larger drops. If the drops and the suspending medium differ in densities, then the coarsening of droplet sizes causes emulsion creaming or sedimentation in the presence of gravity, and eventually, complete phase separation (as indicated in Fig. 2). Droplets in emulsions can move relative to each other due to Brownian motion, gravity and applied mechanical forces (e.g. centrifugation). In this process, they can undergo collisions with each other, during which droplet coalescence can occur. However, only a fraction of all collisions lead to a coalescence event. The rate of coarsening of an emulsion due to coalescence, therefore, depends on two factors: 1) the number of collisions per unit time experienced by the drops, and 2) the likelihood of a collision to lead to coalescence [139]. The former depends on the drop volume fraction, the sizes and spatial distribution of drops, and the flow conditions, which are macroscopic variables. The probability of a collision to lead to coalescence, also referred to as the collision efficiency, is dependent on microscale phenomena, and in particular, on the dynamics associated with the thin film of suspending fluid trapped between two drops when they experience a collision [34,139,140]. The collision efficiency is, therefore, a variable directly integrable into a macroscale, population balance model [139,141,142] that can determine the evolution of drop

size distributions. However, to determine the microscale thin film dynamics and hence the collision efficiency, experiments need to be performed at the level of a few (typically two) drops. Microfluidic platforms are ideally suited for such measurements, and consequently, the majority of microfluidic studies to date have focused on probing the collision efficiency of two drops to lead to coalescence. To understand the collision process and the factors that govern its efficiency to coalescence, we need to understand the various stages in a collision [34,140,143–147]. First, drops approach each other under the influence of hydrodynamic, gravitational, Brownian, or other body/surface forces, and this leads to the sandwiching of a thin film of suspending fluid between the drops. As the two drops are pushed closer to each other by the force, the film drains, and the pressure in the thin film increases due to the decrease of the radius of the thin film region that is proportional to the square root of the film thickness for a film between two spherical drops. If the contact lasts long enough, the film can deform into a dimpled shape as the pressure in the film becomes comparable to the Laplace pressure [140,146]. Eventually, the thin film can be drained to a critical thickness where non-hydrodynamic or disjoining stresses dominate the drainage process [34,62,148–152]. If the disjoining stresses are purely attractive in nature, e.g. due to van der Waals attraction, which can happen for identical drops when the interface is devoid of surfactants or other material that can inhibit coalescence, the film drains rapidly and ruptures, and this causes the two droplets to merge. The more common scenario is that the disjoining stress is repulsive in nature, and the film between the two drops reaches a stable thickness, governed by a balance between the applied force and the separation dependent repulsive force experienced by each drop. Such a film is termed as a black film or a Newtonian black film, depending on the separation [148,150,151]. After this point, the black film can undergo stochastic shape changes due to thermal fluctuations, which can lead to the rupture of the film and coalescence.

The total time of coalescence upon a collision is the sum of time spent in each of the above stages. Several models are available in the literature for the duration of the hydrodynamic drainage phase, t_D [145,146,153,154] and these predict t_D as a function of the applied force causing the drops to approach each other, the IFT, Marangoni stresses (see section 2.1), disjoining stresses, and the shape of the film. The presence of surfactant molecules at the interface can have complex effects on the hydrodynamic drainage of the film. Surfactants can lower the IFT and lead to larger deformations and dimpled thin films for the same contact force, which prolong the hydrodynamic drainage phase. Also, the outgoing flow in the film during drainage sweeps the surfactant molecules away from the center towards the edge of the film, which creates an IFT gradient. Consequently, Marangoni stresses, acting to push fluid from regions with lower IFT towards higher IFT, are imposed at the interface, which leads to reduction in interface mobility and the drainage rate [49,140,155]. However, above the CMC, surfactants can remobilize the interface, provided that they have fast adsorption-desorption kinetics [156–158]. As the flow sweeps away the surfactant monomers towards the edges of the film, there is a depletion of surfactant in the portions of the interface near the center of the film, and an enrichment near the film edge. If the adsorption-desorption kinetics are rapid, the surfactants in the medium near the center of the film repopulate the depleted interface quickly, and the excess surfactants at the edge of the film are immediately desorbed. This produces an equilibrium interface concentration and hence, interfacial tension, which results in the suppression of the Marangoni stress and a remobilization of the interface.

After a stable film is formed, the film rupture time may be estimated based on the *hole nucleation theory* [20]. The activation energy, E_a, is defined as the minimum energy that is required for the formation and expansion of a hole between two adjoining drops. E_a for an emulsion system depends on the film thickness, the IFT [20] [22], the interfacial rigidity [22], and disjoining stresses due to electrostatic [159], van der Waals, and solvation/ structuring effects [151,160]. The IFT and rigidity can be estimated within the HLD – NAC framework for surfactants [59,147], alluded to earlier in this review (section 2.3), and depend on the type of surfactant, the medium chemistry, temperature, etc. As an example, for the right combination of surfactant, oil phase and aqueous phase, if the HLD is close to 0 (near the phase inversion point), the IFT can be small enough to lead to low activation energies. Since the time for film rupture is an exponential function of the activation energy, coalescence can be rapid near the phase inversion point. The longer the contact time between two droplets, the higher the probability of their coalescence. In fact, the coalescence time relative to the contact time can be viewed an indicator of emulsion stability [24,139].

Like surfactants, particles can also stabilize the emulsions (Pickering emulsions) provided that they accumulate on the interface at a sufficiently large area fraction [161–163]. The level of stabilization is primarily controlled by two interfacial mechanisms: ‘jamming’ and ‘bridging’. The former depends on the interfacial coverage and the size of particles. Depending on the interfacial coverage of the particles [164], drops can experience full coalescence (droplets merge to form a larger spherical drop), arrested coalescence (droplets merge, but the drop cannot relax back to a sphere), and full stabilization (droplets do not merge). Arrested coalescence occurs because of the repulsive force between the particles during the process of film rupture. As the drop formed by two merged droplets relaxes, the interfacial area reduces, but the particles cannot desorb and are jammed; this leads to creation of immobile interface [164]. Bridging occurs when a particle is simultaneously adsorbed at the interfaces of two drops, and can stabilize the drops against coalescence if two conditions are met. First, the particles are preferentially wetted by the continuous phase. Second, particle surface fractions are high enough, so that the particle-free regions do not promote coalescence [165]. In contrast, particles which are preferentially wetted by the dispersed phase are known to increase the coalescence rate [165–167]. Finally, nanoparticles that have adsorbed polymeric surfactant components exhibit significant stabilization at concentrations much lower than that observed for nanoparticles or surfactants alone [168]. Wetting of the particles by the continuous phase, along with the electrostatic and dipole repulsion induced by charged polymeric chains, lead to increased stability of an emulsion.

4.2.1. *Coalescence during droplet generation in a microfluidic device*

Microfluidic systems integrated with a high-speed imaging camera allow the investigation of droplet coalescence behavior in dynamic conditions, whereby emulsion stability at small time scales and the impact of different factors on emulsion stability can be screened prior to actual production. The common configurations employed for coalescence studies include T-junction, Y-junction, co-flowing or flow-focusing microfluidic devices where monodisperse droplets are generated. An interesting approach to achieve better control over coalescing drops was developed by Gunes et al. (2013) [169] where multiple, lateral channels are positioned downstream of the drop generation point. The separation between the drops was controlled by either injecting or drawing the liquid out of these equally spaced side channels. Utilization of microfluidic systems to investigate the coalescence behaviors of droplets offers many advantages over the conventional bulk measurement methods. They allow precise control of the factors that affect coalescence (shear rate, medium chemistry, drop size), and provide a direct visualization of the coalescence event. In microfluidic systems, droplet coalescence can be passively and actively investigated, depending on the microchannel geometry and the forces inducing droplet-droplet collisions and coalescence efficiency (e.g. electric or thermal field activation), respectively. There is a substantial number of research studies dedicated to droplet coalescence techniques for a variety of applications, and several excellent reviews have been reported [8,10,13,14,66]. However, there are very limited reviews of this phenomenon in food emulsions. In the following section, various microfluidic systems that investigate the droplet coalescence features of different emulsion types (such as O/W, W/O and Pickering), relevant to food fields, are

presented. A summary of such attempts dedicated to the investigation of droplet coalescence using microfluidic systems is presented in Table 3.

Bremond et al. (2008) [170] investigated coalescence of a pair of isolated droplets (water in hexadecane) generated in a flow focusing geometry and passed through a larger symmetrical coalescence chamber in which a sequence of events including collision, relaxation, separation and fusion of droplet pair was analyzed. Results revealed that the collision of droplet pairs did not cause coalescence. The study also showed that the fast separation of contacting droplets can induce a significant negative hydrodynamic lubrication pressure, which can lead to a local attraction and the formation of two opposing nipples in the contact area, thus facilitating the coalescence (fusion) of droplets. This confirmed prior work on the occurrence of coalescence during the extensional phase of interaction between drops [140,153]. These characteristics were observed for droplet pairs stabilized with and without an emulsifier (e.g. Span 80). For a densely-packed droplet train, the fusion of a droplet pair at one side initiated the coalescence of neighbouring droplets (Fig. 6a). In addition, these results were highly comparable to the theoretical model for the time-dependent droplet deformation due to droplet separation developed by Lai et al. (2009) [190], and were also confirmed in the studies by Gunes et al. (2008, 2010) [191,192] for water droplets in sunflower oil with larger droplet

Table 3
A summary of several studies on the coalescence of droplets using microfluidic systems.

Emulsion characteristics			Microfluidic device characteristics		Investigated coalescence behaviors	References
Type	Dispersed phase	Continuous phase	Droplet formation	Coalescence chamber		
W/O	Water	Hexadecane	Flow focusing junction	Symmetrical coalescence chamber	A droplet pair (stabilized with and without Span 80) and compact system of droplets under flow	[170]
	Water	Silicone oil	Two upstream T- junctions	Downstream T-junction	A droplet pair as a function of droplet sizes and speeds	[171]
	Water Glycerol	Silicone oil	Flow focusing junction	Downstream diamond coalescence chamber	Multiple droplets as a function of flow rate and viscosity	[172]
O/W	Fluorinated oil	Buffered solution (10 mM Tris-HCl)	Flow focusing junction	Rectangular coalescence chamber	Multiple droplets as a function of concentrations and adsorption kinetics of an emulsifier via droplet size distribution determination	[173]
	Hexadecane	Water	Two side-stream T-junctions	Rectangular coalescence chamber where droplets from two symmetrical sides collide	Multiple droplets without emulsifier as a function of droplet concentrations and velocity via coalescence time determination	[174]
	Mineral and silicone oils	Water				[175]
	Mineral oil	NaCl solution				[176]
	Hexadecane	Water	T-junction	A meandering channel and coalescence microchannel	Multiple droplets as a function of Sodium dodecyl sulphate (SDS) and NaCl concentrations via droplet size distribution determination	[177]
					Multiple droplets as a function of types, concentrations, adsorption time of food-grade proteins, and pH levels	[178]
	Heptane, dodecane and xylene	Water	T-junction	A meandering channel, a wider channel, two split channels, and square coalescence chamber	Hundreds or thousands of individual droplet interactions under effects of salinity, oil phase composition, droplet size, concentration of emulsifier and temperature and approach velocity) via coalescence times, also contact times and approaching velocities	[179]
	Hexadecane	Water	Valve-based flow focusing junction	Long serpentine channel	Partial coalescence of droplets during a cooling-heating cycle	[180]
	Silicone oils	Water-glycerol, and C_{12}TAB and C_{16}TAB*	Flow focusing junction	A wide channel	Droplet pairs as a function of emulsifier concentrations and adsorption times	[181]
O/W	Decane, hexadecane and Span 80	Water, salt and SDS			Droplet pairs as a function of types and concentrations of emulsifiers and inorganic salts, and continuous and dispersed phase velocities	[182]
W/O	Water, salt and SDS	Decane, hexadecane and Span 80				
Pickering	Sunflower oil and colloidal lipid particle dispersion	Water	T-junction	A meandering channel and a coalescence microchannel	Multiple droplets as a function of nanoparticle coverage	[183]
	Dodecane	Water, polystyrene nanoparticles and KCl	*Co*-flow geometry	An adsorption channel and a coalescence chamber	Multiple droplets as a function of diffusion-limited particle adsorption (particle size, particle concentration, surface chemistry and ionic strength)	[184]
	Water	n-pentanol and polystyrene nanoparticles	Two side-stream T-junctions	Rectangular coalescence chamber where droplets from two symmetrical sides collide	A droplet pair as a function of particle size and concentration	[167]
	Water and silica microspheres	Miglyol 840	Flow focusing junction	Hyperbolic contraction	Deformation of droplets stabilized by particles	[185]
	Benzyl benzoate	Water and thermo-responsive PNIPAM microgels**	Y-junction	Coalescence chamber	Thermally triggered coalescence of a droplet pair stabilized by particles	[186]
	Dodecane	Water and silica nanoparticles	Flow focusing junction	Rectangular coalescence chamber	Multiple droplets as a function of nanoparticle coverage concentrations	[187]
W/O	Water	Mineral oil and Span 80	Flow focusing junction	A rectangular coalescence chamber integrated with heating wire	Temperature-induced coalescence of a droplet pair as a function of flow rate ratio of dispersed and continuous phase and total flow rate	[188]; [189]

*C_{12}TAB: Dodecyltrimethylammonium bromide, C_{16}TAB: Hexadecyltrimethylammonium bromide.
**PNIPAM: Poly(N-isopropylacrylamide).

and microfluidic channel sizes. Similarly, collision behaviors of a droplet pair over a wide range of droplet sizes and speeds in a microfluidic T-junction were also reported by Christopher et al. (2009) [171]. Three primary collision events (coalescence, slipping and splitting) were recorded depending on the droplet sizes and moving speeds. Coalescence of a droplet pair happened only at low collision speeds. At high collision speeds, droplets with small sizes separated away from each other without merging, while large droplets split into multiple segments. These observations also allowed the development of a stability diagram describing the flow conditions and droplet shape in which each of these collision events occurred.

The coalescence behavior of emulsions with a high dispersed phase fraction as a function of concentrations and adsorption times of an emulsifier (accomplished by changes in delay time between formation and collision of droplets) could be quantified via the determination of the increased sizes of droplets colliding and exiting from a rectangular coalescence cross-slot. The droplet coalescence probability was found to decrease with increasing emulsifier concentrations and was governed by adsorption kinetics of emulsifier [173]. This approach was then extended for studying the coalescence behaviors of droplets stabilized by peptides [193], polymers [194] and even nanoparticles [187]. However, these studies did not consider the drainage dynamics of the thin film of the continuous phase between droplets, which, in some cases, can be the rate determining step of coalescence. To account for the film drainage profile, Kerbs et al. (2012a, 2013, 2012b) [174–176] employed a coalescence microchannel to determine coalescence times of droplets in O/W emulsions (e.g. hexadecane in water, mineral and silicone oils in water, and silicone oils in NaCl solution) as functions of capillary numbers (e.g. droplet velocity) and their viscosities (e.g. droplet concentration). They found that for capillary numbers below 10^{-3}, drainage time reduces with increasing capillary number. This trend appears to be opposite to many hydrodynamic drainage studies proposed in the past [49,140,145,195], where the drainage time increases with capillary number for low capillary numbers. It is important to note, however, that these theories were developed assuming that the film pressure is of the order of the Laplace pressure. For large capillary numbers, the collision between two drops leads to more deformation, greater volume trapped in the film, and hence a retardation of the drainage rate. On the other hand, for capillary numbers below 10^{-3}, where drops collide more gently with negligible deformation, increasing the hydrodynamic force does indeed induce faster hydrodynamic drainage.

Similar results were also reported by Jose et al. (2012) [172] for the coalescence behaviors of droplets of glycerol-water mixtures in silicone oil, in the absence of surfactants. They employed a different microfluidic system that included a droplet generating, flow focusing junction and diamond-shape merging chamber with a size 20 times larger than the channels. Recently, these results were used to develop the model for droplet coalescence kinetics using population balances [196].

For an oil-in-water emulsion with surfactants, Krebs et al. (2012) [177] reported another microfluidic circuit in which droplets (hexadecane in water) were produced in a T-junction, and then underwent collision and coalescence in a wide channel, to determine stability of droplets against coalescence as a function of sodium n-dodecyl sulphate (SDS) and NaCl bulk concentrations. The extent of coalescence was quantified from the mean size differences of droplets initially generated and those at the end of collision chamber. Droplet coalescence did not occur at SDS concentrations higher than 10^{-7} M. Also, the presence of NaCl in the emulsion system (0.1–0.3 M) reduced the thickness of electric double layer between two droplets, thus facilitating coalescence. This microfluidic system was then employed to evaluate the effects of concentration, type, and adsorption time of different protein emulsifiers

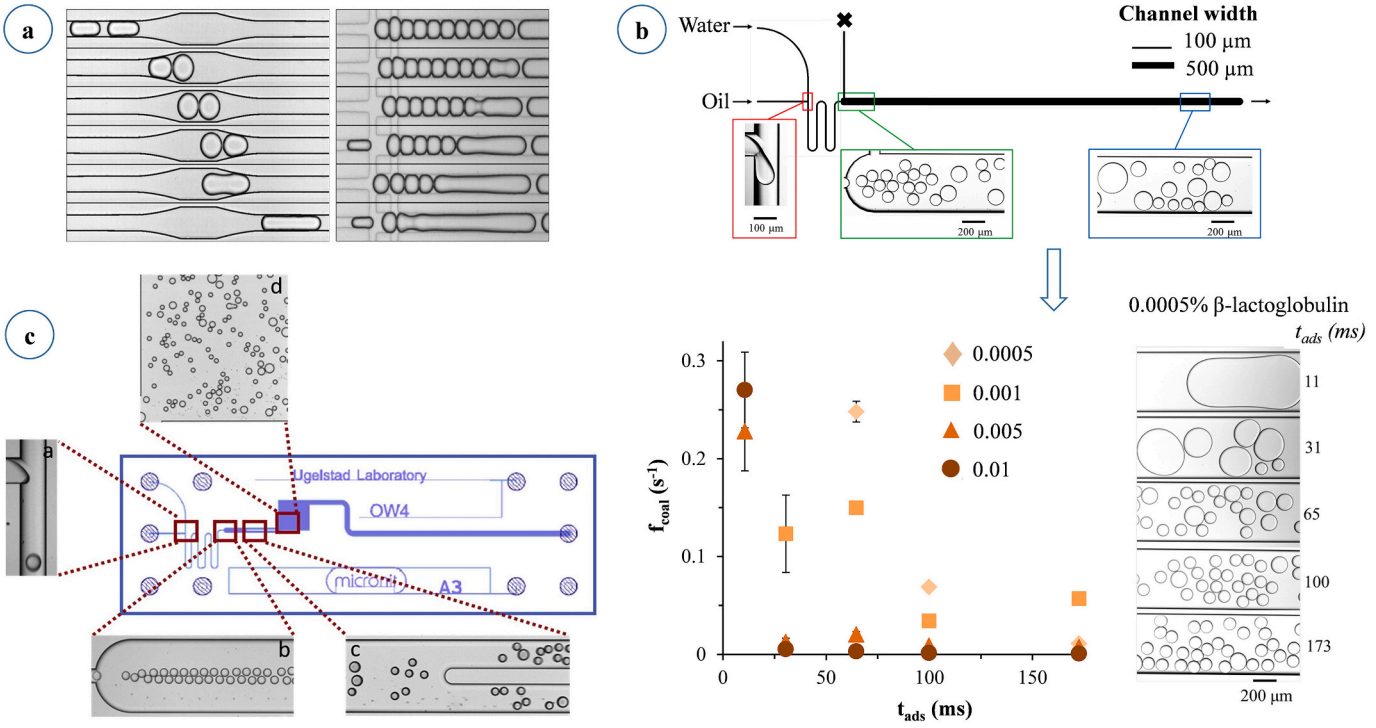

Fig. 6. (a): Collision, separation and recontacting of two droplets demonstrating that coalescence occurred only when droplets were separated (on the left), and a cascade of coalescence events in a compact droplet system, where coalescence of a droplet pair at one end initiated the coalescence of neighbouring droplets driven towards each other by capillary stresses (Adapted with permission from Bremond et al. (2008) [170]). **(b)**: Layout of the microfluidic chip consisting of T-junction for droplet formation, a meandering channel and a wider coalescence channel, and coalescence frequency as a function of the adsorption time with various concentrations of β-lactoglobulin (above image), together with microscope images from the outlet of the coalescence channel for 0.0005% β-lactoglobulin (below image) (Adapted with permission from Muijlwijk et al. (2017) [178]). **(c)**: Sketch of microfluidic chip including a T-junction, a meandering channel, a wider channel, a split channel, and a coalescence chamber where the coalescence time measurements were taken (Adapted with permission from Dudek et al. (2020) [179]).

(e.g. β-lactoglobulin, whey protein isolate, and oxidised whey protein isolate), and pH levels on coalescence stability of hexadecane-in-water emulsions [178]. These studies based on microfluidic techniques represent a significant step towards industrially relevant food-grade emulsion applications. They showed that the proteins that are able to form a homogeneous interface (e.g. β-lactoglobulin) protected droplets against coalescence better than heterogeneous interfacial counterparts (e.g. whey protein isolate and oxidised whey protein isolate). The adsorption time was dependent on the protein concentration, and proteins were unable to stabilize the droplets at pH levels around their isoelectric point (Fig. 6b). Similar effects of types and concentrations of emulsifier, and types and concentrations of inorganic salts, continuous and dispersed phase velocities (determining adsorption times of emulsifier) on the prevention of droplet coalescence were also reported with a different microfluidic geometric system [181,182].

While the aforementioned studies investigated coalescence dynamics of droplets via determination of coalescence time, Dudek et al. (2020) [179] introduced a novel microfluidic chip (see Fig. 6c) to determine not only coalescence times, but also contact times and approach velocities between the droplets for varying salinities of the water phase, oil phase compositions, droplet sizes, emulsifier concentrations and temperatures. With the ability to follow and detect thousands of coalescence events of varied droplet sizes in flow, this system is a highly versatile tool for analysing coalescence dynamics of emulsion droplets. Moreover, microfluidic systems can be designed to determine partial coalescence of droplets. Abedi et al. (2019) [180] employed a valve-based flow-focusing device which is connected to a long serpentine channel, which all are enclosed within a thermal stage to investigate destabilization of hexadecane droplets in water during thermal cycle. It was found that destabilization of emulsions was caused by several simultaneous coalescence events, which yielded small-scale structures first, followed by large-scale structures due to coalescence propagation, and this process accelerated as the droplet size increased.

The mechanism of emulsion stabilization by particles (Pickering emulsions) has been discussed in the section 4.2 As mentioned before, pickering emulsions are stable to coalescence provided that the particles are preferentially wetted by the continuous phase liquid, and their surface concentration is sufficiently high. However, if droplets are brought to contact at the early stages of their formation, the particle surface coverage is not adequate to prevent coalescence. Priest et al. (2011) [187] utilized a flow focusing junction device to generate oil droplets in water in the presence of silica nanoparticles, and collected them downstream after particles equilibrated at the interface. They found that silica nanoparticles did not affect the formation kinetics and sizes of droplets, but stabilized droplets against coalescence. Similar studies using different microfluidic systems (e.g. T-junction and co-flow geometry devices) for Pickering emulsion droplets stabilized by polystyrene nanoparticles [167,184], and for those stabilized by colloidal lipid particle dispersion [183] were also found. They demonstrated that the critical surface particle coverage for preventing the coalescence of particle-stabilized droplets was dependent not only on the nanoparticle concentration, but also on the nanoparticle size and surface chemistry, ionic strength of continuous phase, and confinement level of droplets. For oil droplets in water, hydrophilic nanoparticles were found to promote coalescence whereas hydrophobic nanoparticles protected droplets from coalescing due to additional hydrodynamic resistance to the thin film layer between the approaching droplets. It was also reported that strong confinement of particle-stabilized droplets of water dispersed in oil led to the extreme deformation of droplets, which resulted in their instability [185]. Also, confinement of droplets under shear flow was found to promote coalescence [197], due to a modification of the flow field around the droplets that enhances the inter-droplet interaction time.

In many food applications, understanding the effect of temperature on coalescence rates and emulsion stability is critical. Microfluidic systems in which droplet coalescence is controlled by temperature have also been reported [188,189]. After being generated in a flow-focusing junction, droplets are directed to a coalescence chamber integrated with a heating wire that can be used to heat the emulsion in the chamber to temperatures up to 60 °C by changing the voltage applied to the wire. Studies on Span 80-stabilized water droplets on mineral oil at different temperatures show that the decrease of continuous phase viscosity and interfacial tension, and the increase of thermocapillary forces at high temperatures led to droplet merging. In addition, advances in microfluidic technology have also allowed the generation, pairing and coalescence of droplets with distinct sizes and contents. Coalescence of Pickering emulsions stabilized by thermo-responsive poly (N-isopropylacrylamide) microgels have been studied in microfluidic chips where drops are brought to the heating chamber. In the heating chamber, microgels shrink and consequently reduce the interfacial coverage, which lead to destabilization and coalescence.

Recently, hydrodynamic trap MEFDs have been used to study the coalescence of two drops using two stagnation points [198,199]. The geometry and the fundamentals of these devices are very similar to the ones used by others [127,136] to measure the IFT. However, the new feature is the addition of one more flow inlet and outlet (a total of 6 ports), which introduces two stagnation points. The analytical solution of the flow field has been combined with the "Model Predictive Control" optimization method to constantly update the flow rates such that the stagnation points are always positioned around the droplets to drive them along prescribed trajectories. The study demonstrates the capability of the six port MEFD to precisely collide two Hele-Shaw drops. This is particularly important as the effects of the collision angle and drops offset on the drainage rate are not fully understood for strongly confined droplets, which are frequently encountered in emulsion microfluidics. Moreover, in the studies where characterization of a surfactant is of the interest, drops can be manipulated inside the MEFD long enough to allow the surfactant to equilibrate with the interface, so any uncertainties that may arise due to incomplete coverage of the interface can be eliminated. These are avenues of research currently being explored by the group.

4.2.2. *Coalescence during emulsion storage*

As compared to the number of microfluidic studies on droplet coalescence during emulsion processing, those for emulsions during storage are very limited with only two reported studies [200,201]. In these studies, a microfluidic strategy was introduced for investigating droplet compression and coalescence under centrifugation at the level of individual droplets. This is claimed to be relevant to the accelerated stability testings for emulsions at large scale [1], thus could potentially be used as an analytical approach to predict the long-term stability of monodispersed emulsions. In this system, a sample holder containing a dead-end and rectangular cross-section channel is mounted in a customized-design microcentrifuge, which is placed under an optical microscope integrated with high-speed camera. Nearly monodisperse droplets prepared using T-junction microfluidic device are pumped into the channel, where they exist as a monolayer due to channel shallowness. The behavior of droplets under applied centrifugal forces is then imaged. Droplet-droplet coalescence dynamics of hexadecane-in-water emulsion stabilized by SDS, and of a silicone oil-in-water emulsion stabilized by a thermoresponsive surfactant at different temperatures using a microfluidic microcentrifugation method were investigated by Krebs et al. (2013) [200] and Feng et al. (2015) [201], respectively. Results from both studies indicated that droplet-droplet coalescence occurred only when the local pressure applied to the droplets exceeded the critical disjoining pressure, π_{cr} (e.g. the restoring pressure acting on the droplets when the thin liquid film between two approaching droplets becomes thinner), and the extent of pressure difference determined the coalescence modes. Coalescence happens throughout the bulk of emulsions at relatively low π_{cr}, but only at the front where emulsions meet the bulk of dispersed phase at high π_{cr}. By using a thermoresponsive surfactant with a well-defined "*lower critical solution temperature*" (LCST), the

dependences of π_{cr} on temperature and subsequent droplet coalescence were also investigated [201]. π_{cr} declined significantly at temperatures higher than LCST and vice versa. From the results, it can be inferred that an emulsion prepared at an applied pressure level in the range between π_{cr} at room temperature and π_{cr} at LCST will be stable at room temperature, and increasing temperature to level that cause π_{cr} to decrease while maintaining the applied pressure resulted in rapid destabilization. It must be noted that centrifugation studies will, in general, underpredict the coarsening time. Centrifugation increases the contact force on the droplets, and as explained below, larger contact forces lead to thinner films. The coalescence time is exponentially related to the thin film thickness if interfacial elasticity effects are negligible [22,59,202], and hence, thinner films lead to shorter coarsening times. Centrifugation can also lead to increased deformation of the drops, which, in the case of Pickering emulsions, dilutes the particle concentration at the interface and may promote quicker coalescence. However, under real storage conditions where the contact forces and drop deformation are weaker, the coalescence times can be significantly larger. The details of the relationship of the disjoining stress with the thin film thickness and the mechanical properties of the interface are necessary to establish the coalescence time correctly.

Goel et al. (2018) [202] studied the coalescence of two water droplets in an oil (bitumen solution) in a head on configuration by a method similar to the micropipette aspiration technique, but performed in a confinining microfluidic channel. Droplets were produced at the tip of two microcapillary tubes introduced from two opposite channels inside a cross-slot microfluidic configuration, and the channel was flooded with the oil flowing in and out of the other opposite pair channels of the cross-slot. One microcapillary tube was moved with a linear stage and the drop at its end was contacted with the drop on the other microcapillary at different pressures, and the time to coalescence was recorded. The study showed that if drops are pushed against each other with a large enough contact pressure and for an adequate contact time, coalescence can eventually occur. They obtained an exponential relationship between the contact pressure and the drainage time, which they attributed to be governed by the hole nucleation time that has an inverse exponential dependence on the film thickness.

5. Conclusion and future perspectives for food applications

This study reviews the state-of-the-art in microfluidics to produce, analyze, and characterize emulsions, due to their importance in pharmacy, food processing, cosmetics, and bioengineering. The diversity in the materials and fabrication methods of microfluidic devices, along with the implementation of analytical techniques, such as interfacial and flow induced force balances make microfluidics a unique platform for the measurement of important properties of emulsions. These properties include the dynamic and equilibrium IFT, adsorption-desorption kinetics of the emulsifiers at the interfaces, and the breakup and coalescence rates of the drops. Analyzing these properties using microfluidic devices offers many advantages over conventional macroscopic methods, including the smaller sample requirement, short time-scale measurements, more precise control over the flow conditions and direct visualization. Note that despite their strengths, in many cases, the results of microfluidic experiments need to be coupled with other microscopy and force measurement techniques such as interferometry, electron microscopy and atomic force microscopy to produce a more comprehensive understanding. Examples of this can be seen in thin film experiments where the interferometric techniques have been implemented to estimate the film drainage rate, or to observe the arrangement of surface-active species at the interface using atomic force microscopy.

In foods, the application of microfluidic systems has been limited so far to the preparation of emulsions with accurate control over the droplet size and shape. However, microfluidics has great potential to be a bench-scale analytical technique for the measurement of the rheological and stability properties of emulsions, as well as for the design and characterization of new emulsifiers. Although the sizes of droplets generated in the reported microfluidic systems range between a few microns to a few hundreds of microns, rapid advances of nanotechnology and nanofabrication have paved the way for the development of custom-designed and food-compatible microfluidic systems to study the interfacial properties of both micro- and nanoemulsions. The insights gained through these studies will be invaluable for designing and tailoring emulsion-based delivery systems for bioactive compounds.

Declaration of Competing Interest

None.

Acknowledgments

The authors acknowledge the Academy of Finland (project No. 322514) for funding. The authors also are thankful to Julia Varis for drawing the graphical abstract, and to Mr. Troy Faithfull for his proofreading. Prof. Ramchandran acknowledges the Canada Research Chair program (File# 950-231567) and the NSERC Discovery Grant (File# 402005) that funded this work.

References

[1] McClements DJ. Critical review of techniques and methodologies for characterization of emulsion stability. Crit Rev Food Sci Nutr 2007;47(7):611–49.
[2] Schmitt V, Leal-Calderon F, Bibette J. Preparation of monodisperse particles and emulsions by controlled shear. In: Antonietti M, editor. Colloid chemistry II. Berlin: Springer Verlag GmbH; 2003. p. 195–215.
[3] Wang L-Y, Ma G-H, Su Z-G. Preparation of uniform sized chitosan microspheres by membrane emulsification technique and application as a carrier of protein drug. J Control Release 2005;106(1–2):62–75.
[4] Cameron, J.C., Fischer, C.A., Lehman, N.C., Lindquist, J.S., Olson, C.E., and Fox, S.A., Hot melt adhesive pellet comprising continuous coating of pelletizing aid. 2000, International Patent: WO 99/18147.
[5] Comunian TA, Jafari SM. Production of food bioactive-loaded nanostructures by Micro-/Nanofluidics. In: Jafari SM, editor. Nanoencapsulation of food ingredients by specialized equipment. London: Elsevier; 2019. p. 213–50.
[6] Sugiura S, Nakajima M, Kumazawa N, Iwamoto S, Seki M. Characterization of spontaneous transformation-based droplet formation during microchannel emulsification. J Phys Chem B 2002;106(36):9405–9.
[7] Liu Y, Li Y, Hensel A, Brandner JJ, Zhang K, Du X, et al. A review on emulsification via microfluidic processes. Front Chem Sci Eng 2020:1–15.
[8] Feng S, Yi L, Zhao-Miao L, Ren-Tuo C, Gui-Ren W. Advances in micro-droplets coalescence using microfluidics. Chin J Anal Chem 2015;43(12):1942–54.
[9] Skurtys O, Aguilera J. Applications of microfluidic devices in food engineering. Food Biophys 2008;3:1–15.
[10] Engl W, Backov R, Panizza P. Controlled production of emulsions and particles by milli-and microfluidic techniques. Curr Opin Colloid Interface Sci 2008;13(4):206–16.
[11] Muijlwijk K, Berton-Carabin C, Schroën K. Cross-flow microfluidic emulsification from a food perspective. Trends Food Sci Technol 2016;49:51–63.
[12] Shah RK, Shum HC, Rowat AC, Lee D, Agresti JJ, Utada AS, et al. Designer emulsions using microfluidics. Mater Today 2008;11(4):18–27.
[13] Anna SL. Droplets and bubbles in microfluidic devices. Annu Rev Fluid Mech 2016;48:285–309.
[14] Bremond N, Bibette J. Exploring emulsion science with microfluidics. Soft Matter 2012;8(41):10549–59.
[15] Muijlwijk K, Berton-Carabin C, Schroën K. How microfluidic methods can lead to better emulsion products. Lipid Technol 2015;27(10):234–6.
[16] Maan AA, Nazir A, Khan MKI, Boom R, Schroën K. Microfluidic emulsification in food processing. J Food Eng 2015;147:1–7.
[17] Gunes DZ. Microfluidics for food science and engineering. Curr Opin Food Sci 2018;21:57–65.
[18] Berton-Carabin CC, Schroën K. Pickering emulsions for food applications: background, trends, and challenges. Annu Rev Food Sci Technol 2015;6:263–97.
[19] Tucker III CL, Moldenaers P. Microstructural evolution in polymer blends. Annu Rev Fluid Mech 2002;34(1):177–210.
[20] De Vries A. Foam stability: part IV. Kinetics and activation energy of film rupture. Recueil des Travaux Chimiques des Pays-Bas 1958;77(4):383–99.
[21] Vrij A. Possible mechanism for the spontaneous rupture of thin, free liquid films. Discuss Faraday Soc 1966;42:23–33.
[22] Acosta EJ, Le MA, Harwell JH, Sabatini DA. Coalescence and solubilization kinetics in linker-modified microemulsions and related systems. Langmuir. 2003;19(3):566–74.
[23] Abbott S. Surfactant Science: Principles and Practice. Creative commons. http://www.stevenabbott.co.uk/practical-surfactants/the-book.php; 2016 (Accessed by 8 December 2020).

[24] McClements DJ. Food emulsions: Principles, practices, and techniques. New York: CRC press; 2015.
[25] Tadros TF. Emulsions: Formation, stability, industrial applications. Berlin: Walter De Gruyter; 2016.
[26] McClements DJ, Jafari SM. Improving emulsion formation, stability and performance using mixed emulsifiers: a review. Adv Colloid Interf Sci 2018;251:55–79.
[27] Wong S, Lim J, Dol S. Crude oil emulsion: a review on formation, classification and stability of water-in-oil emulsions. J Pet Sci Eng 2015;135:498–504.
[28] Fingas M. Water-in-oil emulsion formation: a review of physics and mathematical modelling. Spill Sci Technol Bull 1995;2(1):55–9.
[29] Leal-Calderon F, Schmitt V, Bibette J. Emulsion science: Basic principles. New York: Springer Science & Business Media; 2007.
[30] Van den Tempel M, Lucassen-Reynders E. Relaxation processes at fluid interfaces. Adv Colloid Interf Sci 1983;18(3–4):281–301.
[31] Fuller GG, Vermant J. Complex fluid-fluid interfaces: rheology and structure. Annual Rev Chem Biomol Eng 2012;3:519–43.
[32] Pepicelli M, Verwijlen T, Tervoort TA, Vermant J. Characterization and modelling of Langmuir interfaces with finite elasticity. Soft Matter 2017;13(35):5977–90.
[33] Renggli D, Alicke A, Ewoldt RH, Vermant J. Operating windows for oscillatory interfacial shear rheology. J Rheol 2020;64(1):141–60.
[34] Chatzigiannakis E, Jaensson N, Vermant J. Thin liquid films: where hydrodynamics, capillarity, surface stresses and intermolecular forces meet. Curr Opin Colloid Interface Sci 2021;101441.
[35] Grace HP. Dispersion phenomena in high viscosity immiscible fluid systems and application of static mixers as dispersion devices in such systems. Chem Eng Commun 1982;14(3–6):225–77.
[36] Bentley B, Leal LG. An experimental investigation of drop deformation and breakup in steady, two-dimensional linear flows. J Fluid Mech 1986;167:241–83.
[37] Stone HA. Dynamics of drop deformation and breakup in viscous fluids. Annu Rev Fluid Mech 1994;26(1):65–102.
[38] Suryo R, Basaran OA. Local dynamics during pinch-off of liquid threads of power law fluids: scaling analysis and self-similarity. J Non-Newtonian Fluid Mech 2006;138(2–3):134–60.
[39] Gupta A, Eral HB, Hatton TA, Doyle PS. Nanoemulsions: formation, properties and applications. Soft Matter 2016;12(11):2826–41.
[40] Taylor GI. The formation of emulsions in definable fields of flow. Proceed Royal Soc London Series A 1934;146(858):501–23.
[41] De Bruijn R. Tipstreaming of drops in simple shear flows. Chem Eng Sci 1993;48(2):277–84.
[42] Eggleton CD, Tsai T-M, Stebe KJ. Tip streaming from a drop in the presence of surfactants. Phys Rev Lett 2001;87(4):048302.
[43] Anna SL, Bontoux N, Stone HA. Formation of dispersions using “flow focusing” in microchannels. Appl Phys Lett 2003;82(3):364–6.
[44] Anna SL, Mayer HC. Microscale tipstreaming in a microfluidic flow focusing device. Phys Fluids 2006;18(12):121512.
[45] Moyle TM, Walker LM, Anna SL. Predicting conditions for microscale surfactant mediated tipstreaming. Phys Fluids 2012;24(8):082110.
[46] Wang Q, Siegel M, Booty MR. Numerical simulation of drop and bubble dynamics with soluble surfactant. Phys Fluids 2014;26(5):052102.
[47] Sonthalia R, Ng S, Ramachandran A. Formation of extremely fine water droplets in sheared, concentrated bitumen solutions via surfactant-mediated tip streaming. Fuel. 2016;180:538–50.
[48] Ettahiri A. The generation of extremely fine water-in-bitumen emulsions via the satellite drop formation mechanism. Master thesis. Canada: Department of Chemical Engineering and Applied Chemistry, University of Toronto; 2018.
[49] Hu Y, Pine D, Leal LG. Drop deformation, breakup, and coalescence with compatibilizer. Phys Fluids 2000;12(3):484–9.
[50] Tsai T, Miksis MJ. Dynamics of a drop in a constricted capillary tube. J Fluid Mech 1994;274:197–217.
[51] Rosen MJ, Kunjappu JT. Surfactants and interfacial phenomena. 4th ed. Hoboken, New Jersey: John Wiley & Sons; 2012.
[52] Bankcroft W. The theory of emulsification. J Phys Chem 1913;17.
[53] Griffin WC. Classification of surface-active agents by HLB. J Soc Cosmet Chem 1949;1:311–26.
[54] Salager J, Morgan J, Schechter R, Wade W, Vasquez E. Optimum formulation of surfactant/water/oil systems for minimum interfacial tension or phase behavior. Soc Pet Eng J 1979;19(02):107–15.
[55] Kruglyakov PM. Hydrophile-lipophile balance of surfactants and solid particles: Physicochemical aspects and applications. Amsterdam: Elsevier; 2000.
[56] Acosta EJ. The HLD–NAC equation of state for microemulsions formulated with nonionic alcohol ethoxylate and alkylphenol ethoxylate surfactants. Colloids Surf A Physicochem Eng Asp 2008;320(1–3):193–204.
[57] Acosta E, Szekeres E, Sabatini DA, Harwell JH. Net-average curvature model for solubilization and supersolubilization in surfactant microemulsions. Langmuir. 2003;19(1):186–95.
[58] Acosta E. Modeling and formulation of microemulsions: the net-average curvature model and the combined linker effect. PhD thesis. Japan: School of Chemical Engineering and Materials Science, University of Oklahoma; 2004.
[59] Kiran SK. Application of the HLD and NAC models to the formation and stability of emulsions. PhD Thesis. Canada: Department of Chemical Engineering and Applied Chemistry, University of Toronto; 2013.
[60] Salager J-L, Antón RE. Ionic microemulsions. In: Kumar Promod, Mittal KL, editors. Handbook of microemulsion science and technology. New York: Marcel Dekker; 2018. p. 247–80.
[61] Acosta EJ, Yuan JS, Bhakta AS. The characteristic curvature of ionic surfactants. J Surfactant Deterg 2008;11(2):145–58.
[62] Israelachvili JN. Intermolecular and surface forces. 3rd ed. Oxford, UK: Academic Press; 2011.
[63] Gao T, Rosen M. Dynamic surface tension of aqueous surfactant solutions: 7. Physical significance of dynamic parameters and the induction period. J Colloid Interface Sci 1995;172(1):242–8.
[64] Ferri JK, Stebe K. Which surfactants reduce surface tension faster? A scaling argument for diffusion-controlled adsorption. Adv Colloid Interf Sci 2000;85(1):61–97.
[65] Maan AA, Schroën K, Boom R. Spontaneous droplet formation techniques for monodisperse emulsions preparation–perspectives for food applications. J Food Eng 2011;107(3–4):334–46.
[66] Zhu P, Wang L. Passive and active droplet generation with microfluidics: a review. Lab Chip 2017;17(1):34–75.
[67] Van Dijke KC, Schroën KC, Boom RM. Microchannel emulsification: from computational fluid dynamics to predictive analytical model. Langmuir. 2008;24(18):10107–15.
[68] Sugiura S, Nakajima M, Seki M. Effect of channel structure on microchannel emulsification. Langmuir. 2002;18(15):5708–12.
[69] Kobayashi I, Takano T, Maeda R, Wada Y, Uemura K, Nakajima M. Straight-through microchannel devices for generating monodisperse emulsion droplets several microns in size. Microfluid Nanofluid 2008;4:167–77.
[70] van Dijke KC, Schroën K, van der Padt A, Boom R. EDGE emulsification for food-grade dispersions. J Food Eng 2010;97(3):348–54.
[71] Castillo-León J. Microfluidics and lab-on-a-chip devices: history and challenges. In: Castillo-León J, Svendsen WE, editors. Lab-on-a-Chip Devices and Micro-Total Analysis Systems: A Practical Guide. Cham: Springer International Publishing; 2015. p. 1–15.
[72] Gale BK, Jafek AR, Lambert CJ, Goenner BL, Moghimifam H, Nze UC, et al. A review of current methods in microfluidic device fabrication and future commercialization prospects. Inventions. 2018;3(3):60.
[73] Ren K, Zhou J, Wu H. Materials for microfluidic chip fabrication. Acc Chem Res 2013;46(11):2396–406.
[74] Bhandari P, Narahari T, Dendukuri D. ‘Fab-chips’: a versatile, fabric-based platform for low-cost, rapid and multiplexed diagnostics. Lab Chip 2011;11(15):2493–9.
[75] Agustini D, Bergamini MF, Marcolino-Junior LH. Low cost microfluidic device based on cotton threads for electroanalytical application. Lab Chip 2016;16(2):345–52.
[76] Roy E, Pallandre A, Zribi B, Horny MC, Delapierre FD, Cattoni A, et al. Overview of materials for microfluidic applications. In: Yu X-Y, editor. Advances in microfluidics-new applications in biology, energy, and materials sciences. IntechOpen; 2016.
[77] Song Y, Cheng D, Zhao L. Microfluidics: Fundamentals, Devices, and Applications. Weinheim: Wiley-VCH Verlag GmbH & Co; 2018.
[78] Akyazi T, Basabe-Desmonts L, Benito-Lopez F. Review on microfluidic paper-based analytical devices towards commercialisation. Anal Chim Acta 2018;1001:1–17.
[79] Nielsen JB, Hanson RL, Almughamsi HM, Pang C, Fish TR, Woolley AT. Microfluidics: innovations in materials and their fabrication and functionalization. Anal Chem 2019;92(1):150–68.
[80] Yoon DH, Tanaka D, Sekiguchi T, Shoji S. Structural formation of oil-in-water (O/W) and water-in-oil-in-water (W/O/W) droplets in PDMS device using protrusion channel without hydrophilic surface treatment. Micromachines. 2018;9(9):468.
[81] Kitsara M, Ducrée J. Integration of functional materials and surface modification for polymeric microfluidic systems. J Micromech Microeng 2013;23(3):033001.
[82] Wang Z, Zhang T. Microfluidics devices: fabrication and surface modification. In: Yujun S, Daojian C, Liang Z, editors. Microfluidics: fundamentals, devices, and applications. Weinheim: Wiley-VCH Verlag GmbH & Co; 2018. p. 113–45.
[83] Wong I, Ho C-M. Surface molecular property modifications for poly (dimethylsiloxane)(PDMS) based microfluidic devices. Microfluid Nanofluid 2009;7(3):291–306.
[84] Zhou J, Khodakov DA, Ellis AV, Voelcker NH. Surface modification for PDMS-based microfluidic devices. Electrophoresis. 2012;33(1):89–104.
[85] Makamba H, Kim JH, Lim K, Park N, Hahn JH. Surface modification of poly (dimethylsiloxane) microchannels. Electrophoresis. 2003;24(21):3607–19.
[86] Hu S, Ren X, Bachman M, Sims CE, Li G, Allbritton N. Surface modification of poly (dimethylsiloxane) microfluidic devices by ultraviolet polymer grafting. Anal Chem 2002;74(16):4117–23.
[87] Subramanian B, Kim N, Lee W, Spivak DA, Nikitopoulos DE, McCarley RL, et al. Surface modification of droplet polymeric microfluidic devices for the stable and continuous generation of aqueous droplets. Langmuir. 2011;27(12):7949–57.
[88] Abate AR, Lee D, Holtze C, Krummel A. And do T, W.D. functionalized glass coating for PDMS Microfluidic devices. In: Herold KE, Rasooly A, editors. Lab on a Chip Technology: fabrication microfluidics and Nanofluidics. Norwich: Caister Academic Press; 2009.
[89] Saitoh T, Suzuki Y, Hiraide M. Preparation of poly (N-isopropylacrylamide)-modified glass surface for flow control in microfluidics. Anal Sci 2002;18(2):203–5.
[90] Berdichevsky Y, Khandurina J, Guttman A, Lo Y-H. UV/ozone modification of poly (dimethylsiloxane) microfluidic channels. Sensors Actuators B Chem 2004;97(2–3):402–8.
[91] Almutairi Z, Ren CL, Simon L. Evaluation of polydimethylsiloxane (PDMS) surface modification approaches for microfluidic applications. Colloids Surf A Physicochem Eng Asp 2012;415:406–12.

[92] Kaneda S, Ono K, Fukuba T, Nojima T, Yamamoto T, Fujii T. Modification of the glass surface property in PDMS-glass hybrid microfluidic devices. Anal Sci 2012; 28(1):39–44.
[93] Prakash S, Long TM, Selby JC, Moore JS, Shannon MA. "Click" modification of silica surfaces and glass microfluidic channels. Anal Chem 2007;79(4):1661–7.
[94] Tsougeni K, Vourdas N, Tserepi A, Gogolides E, Cardinaud C. Mechanisms of oxygen plasma nanotexturing of organic polymer surfaces: from stable super hydrophilic to super hydrophobic surfaces. Langmuir. 2009;25(19):11748–59.
[95] Maheshwari N, Kottantharayil A, Kumar M, Mukherji S. Long term hydrophilic coating on poly (dimethylsiloxane) substrates for microfluidic applications. Appl Surf Sci 2010;257(2):451–7.
[96] Jankowski P, Ogonczyk D, Kosinski A, Lisowski W, Garstecki P. Hydrophobic modification of polycarbonate for reproducible and stable formation of biocompatible microparticles. Lab Chip 2011;11(4):748–52.
[97] Hozumi A, Inagaki H, Kameyama T. The hydrophilization of polystyrene substrates by 172-nm vacuum ultraviolet light. J Colloid Interface Sci 2004;278 (2):383–92.
[98] Riche CT, Marin BC, Malmstadt N, Gupta M. Vapor deposition of cross-linked fluoropolymer barrier coatings onto pre-assembled microfluidic devices. Lab Chip 2011;11(18):3049–52.
[99] Bashir S, Bashir M, Rees JM, Zimmerman WB. Hydrophilic surface modification of PDMS microchannel for O/W and W/O/W emulsions. Micromachines. 2015;6 (10):1445–58.
[100] Su S, Jing G, Zhang M, Liu B, Zhu X, Wang B, et al. One-step bonding and hydrophobic surface modification method for rapid fabrication of polycarbonate-based droplet microfluidic chips. Sensors Actuators B Chem 2019;282:60–8.
[101] Ortiz R, Chen JL, Stuckey DC, Steele TW. Poly (methyl methacrylate) surface modification for surfactant-free real-time toxicity assay on droplet microfluidic platform. ACS Appl Mater Interfaces 2017;9(15):13801–11.
[102] Chen Z, Lee JB. Surface modification with gallium coating as nonwetting surfaces for gallium-based liquid metal droplet manipulation. ACS Appl Mater Interfaces 2019;11(38):35488–95.
[103] Trantidou T, Elani Y, Parsons E, Ces O. Hydrophilic surface modification of PDMS for droplet microfluidics using a simple, quick, and robust method via PVA deposition. Microsyst Nanoeng 2017;3(1):1–9.
[104] Lee J-H, Kim SK, Park H-H, Kim TS. TiO_2 coated microfluidic devices for recoverable hydrophilic and hydrophobic patterns. J Micromech Microeng 2015; 25(3):035032.
[105] Dukhin SS, Kretzschmar G, Miller R. Dynamics of adsorption at liquid interfaces: Theory, experiment, application. Amsterdam: Elsevier; 1995.
[106] Drelich J, Fang C, White C. Measurement of interfacial tension in fluid-fluid systems. Encyclop Surface Colloid Sci 2002;3:3158–63.
[107] Whitesides GM. The origins and the future of microfluidics. Nature. 2006;442 (7101):368–73.
[108] Lee S, Kim DH, Needham D. Equilibrium and dynamic interfacial tension measurements at microscopic interfaces using a micropipet technique. 1. A new method for determination of interfacial tension. Langmuir. 2001;17(18):5537–43.
[109] Gu H, Duits MH, Mugele F. Interfacial tension measurements with microfluidic tapered channels. Colloids Surf A Physicochem Eng Asp 2011;389(1–3):38–42.
[110] Zhou H, Yao Y, Chen Q, Li G, Yao S. A facile microfluidic strategy for measuring interfacial tension. Appl Phys Lett 2013;103(23):234102.
[111] Tsai SS, Wexler JS, Wan J, Stone HA. Microfluidic ultralow interfacial tensiometry with magnetic particles. Lab Chip 2013;13(1):119–25.
[112] Hudson SD, Cabral JT, Goodrum Jr WJ, Beers KL, Amis EJ. Microfluidic interfacial tensiometry. Appl Phys Lett 2005;87(8):081905.
[113] Cabral JT, Hudson SD. Microfluidic approach for rapid multicomponent interfacial tensiometry. Lab Chip 2006;6(3):427–36.
[114] Martin JD, Hudson SD. Mass transfer and interfacial properties in two-phase microchannel flows. New J Phys 2009;11(11):115005.
[115] Nguyen N-T, Lassemono S, Chollet FA, Yang C. Interfacial tension measurement with an optofluidic sensor. IEEE Sensors J 2007;7(5):692–7.
[116] Wang K, Lu Y, Xu J, Luo G. Determination of dynamic interfacial tension and its effect on droplet formation in the T-shaped microdispersion process. Langmuir. 2009;25(4):2153–8.
[117] Wang X, Riaud A, Wang K, Luo G. Pressure drop-based determination of dynamic interfacial tension of droplet generation process in T-junction microchannel. Microfluid Nanofluid 2015;18(3):503–12.
[118] Li S, Xu J, Wang Y, Luo G. A new interfacial tension measurement method through a pore array micro-structured device. J Colloid Interface Sci 2009;331(1): 127–31.
[119] Brosseau Q, Vrignon J, Baret J-C. Microfluidic dynamic interfacial tensiometry (μDIT). Soft Matter 2014;10(17):3066–76.
[120] Xu J, Li S, Lan W, Luo G. Microfluidic approach for rapid interfacial tension measurement. Langmuir. 2008;24(19):11287–92.
[121] Muijlwijk K, Hinderink E, Ershov D, Berton-Carabin C, Schroën K. Interfacial tension measured at high expansion rates and within milliseconds using microfluidics. J Colloid Interface Sci 2016;470:71–9.
[122] Güell C, Ferrando M, Trentin A, Schroën K. Apparent interfacial tension effects in protein stabilized emulsions prepared with microstructured systems. Membranes. 2017;7(2):19.
[123] Steegmans ML, Warmerdam A, Schroen KG, Boom RM. Dynamic interfacial tension measurements with microfluidic Y-junctions. Langmuir. 2009;25(17): 9751–8.
[124] Honaker LW, Lagerwall JP, Jampani V. Microfluidic tensiometry technique for the characterization of the interfacial tension between immiscible liquids. Langmuir. 2018;34(7):2403–9.
[125] D'Apolito R, Perazzo A, D'Antuono M, Preziosi V, Tomaiuolo G, Miller R, et al. Measuring interfacial tension of emulsions in situ by microfluidics. Langmuir. 2018;34(17):4991–7.
[126] Lee D, Fang C, Ravan AS, Fuller GG, Shen AQ. Temperature controlled tensiometry using droplet microfluidics. Lab Chip 2017;17(4):717–26.
[127] Goel S, Joshi N, Uddin MS, Ng S, Acosta E, Ramachandran A. Interfacial tension of the water-diluted bitumen interface at high bitumen concentrations measured using a microfluidic technique. Langmuir. 2019;35(48):15710–22.
[128] Narayan S, Moravec DB, Dallas AJ, Dutcher CS. Droplet shape relaxation in a four-channel microfluidic hydrodynamic trap. Phys Rev Fluids 2020;5(11):113603.
[129] Lee D, Shen AQ. Interfacial tension measurements in microfluidic quasi-static extensional flows. Micromachines. 2021;12(3):272.
[130] Chen Y, Dutcher CS. Size dependent droplet interfacial tension and surfactant transport in liquid–liquid systems, with applications in shipboard oily bilgewater emulsions. Soft Matter 2020;16(12):2994–3004.
[131] Yeung A, Dabros T, Masliyah J, Czarnecki J. Micropipette: a new technique in emulsion research. Coll Surf A Physicochem Eng Aspects 2000;174(1–2):169–81.
[132] Hochmuth RM. Micropipette aspiration of living cells. J Biomech 2000;33(1): 15–22.
[133] Lee S, Kim DH, Needham D. Equilibrium and dynamic interfacial tension measurements at microscopic interfaces using a micropipet technique. 2. Dynamics of phospholipid monolayer formation and equilibrium tensions at the water-air interface. Langmuir. 2001;17(18):5544–50.
[134] Kumar D, Shenoy A, Deutsch J, Schroeder CM. Automation and flow control for particle manipulation. Curr Opin Chem Eng 2020;29:1–8.
[135] Chen Y, Narayan S, Dutcher CS. Phase-dependent surfactant transport on the microscale: interfacial tension and droplet coalescence. Langmuir 2020;36(49): 14904–23.
[136] Motagamwala AH. A microfluidic, extensional flow device for manipulating soft particles.. Master Thesis. Canada: Department of Chemical Engineering and Applied Chemistry, University of Toronto; 2013.
[137] Mustafa A, Erten A, Ayaz RMA, Kayıllıoğlu O, Eser A, Eryürek M, et al. Enhanced dissolution of liquid microdroplets in the extensional creeping flow of a hydrodynamic trap. Langmuir. 2016;32(37):9460–7.
[138] Jaensson N, Vermant J. Tensiometry and rheology of complex interfaces. Curr Opin Colloid Interface Sci 2018;37:136–50.
[139] Liao Y, Lucas D. A literature review on mechanisms and models for the coalescence process of fluid particles. Chem Eng Sci 2010;65(10):2851–64.
[140] Leal L. Flow induced coalescence of drops in a viscous fluid. Phys Fluids 2004;16 (6):1833–51.
[141] Chen Z, Prüss J, Warnecke H-J. A population balance model for disperse systems: drop size distribution in emulsion. Chem Eng Sci 1998;53(5):1059–66.
[142] Castellano S, Sheibat-Othman N, Marchisio D, Buffo A, Charton S. Description of droplet coalescence and breakup in emulsions through a homogeneous population balance model. Chem Eng J 2018;354:1197–207.
[143] Frankel S, Mysels KJ. Bursting of soap films. II. Theoretical considerations. J Phys Chem 1969;73(9):3028–38.
[144] Hartland S, Jeelani SAK. Drainage of thin dimpled non-Newtonian fluid films. J Phys Chem 1986;90(22):6054–9.
[145] Chesters AK. Modelling of coalescence processes in fluid-liquid dispersions: a review of current understanding. Chem Eng Res Des 1991;69(A4):259–70.
[146] Ramachandran A, Leal L. Effect of interfacial slip on the thin film drainage time for two equal-sized, surfactant-free drops undergoing a head-on collision: a scaling analysis. Phys Rev Fluids 2016;1(6):064204.
[147] Goel S, Ramachandran A. The suppression of droplet-droplet coalescence in a sheared yield stress fluid. J Colloid Interface Sci 2017;492:199–206.
[148] Edwards D, Brenner H, Wasan D. Interfacial transport processes and rheology. Boston: Butterworth-Heinemann; 1991.
[149] Schramm LL. Suspensions: Fundamental and Applications in the Petroleum Industry. Advances in Chemistry Series. Washington, DC: American Chemical Society; 1996.
[150] Bergeron V. Forces and structure in thin liquid soap films. J Phys Condens Matter 1999;11(19):R215–38.
[151] Stubenrauch C, Von Klitzing R. Disjoining pressure in thin liquid foam and emulsion films-new concepts and perspectives. J Phys Condens Matter 2003;15 (27):R1197–232.
[152] Exerowa D, Gotchev G, Kolarov T, Khristov K, Levecke B, Tadros TJL. Interaction forces in thin liquid films stabilized by hydrophobically modified inulin polymeric surfactant. 2. Emulsion films. Langmuir 2007;23(4):1711–5.
[153] Chan DY, Klaseboer E, Manica R. Film drainage and coalescence between deformable drops and bubbles. Soft Matter 2011;7(6):2235–64.
[154] Janssen P, Anderson P, Peters G, Meijer H. Axisymmetric boundary integral simulations of film drainage between two viscous drops. J Fluid Mech 2006;567: 65–90.
[155] Ha J, Yoon Y, Leal L. The effect of compatibilizer on the coalescence of two drops in flow. Phys Fluids 2003;15(4):849–67.
[156] Stebe KJ, Lin SY, Maldarelli C. Remobilizing surfactant retarded fluid particle interfaces. I. Stress-free conditions at the interfaces of micellar solutions of surfactants with fast sorption kinetics. Physics of Fluids A: Fluid Dynamics 1991;3 (1):3–20.
[157] Stebe KJ, Maldarelli C. Remobilizing surfactant retarded fluid particle interfaces: II. Controlling the surface mobility at interfaces of solutions containing surface active components. J Coll Interface Sci 1994;163(1):177–89.
[158] King MR, Leighton Jr DT. Measurement of shear-induced dispersion in a dilute emulsion. Phys Fluids 2001;13(2):397–406.

[159] Milner ST, Xi H. How copolymers promote mixing of immiscible homopolymers. J Rheol 1996;40(4):663–87.
[160] Zhang Y, Sharma V. Domain expansion dynamics in stratifying foam films: experiments. Soft Matter 2015;11(22):4408–17.
[161] Tambe DE, Sharma MM. The effect of colloidal particles on fluid-fluid interfacial properties and emulsion stability. Adv Colloid Interf Sci 1994;52:1–63.
[162] Berton-Carabin CC, Schroën K. Pickering emulsions for food applications: background, trends, and challenges. Annu Rev Food Sci Technol 2015;6:263–97.
[163] Binks BP. Colloidal particles at a range of fluid–fluid interfaces. Langmuir. 2017; 33(28):6947–63.
[164] Pawar AB, Caggioni M, Ergun R, Hartel RW, Spicer PT. Arrested coalescence in Pickering emulsions. Soft Matter 2011;7(17):7710–6.
[165] Nagarkar SP, Velankar SS. Morphology and rheology of ternary fluid-fluid-solid systems. Soft Matter 2012;8(32):8464–77.
[166] Hunter TN, Pugh RJ, Franks GV, Jameson G. The role of particles in stabilising foams and emulsions. Adv Colloid Interf Sci 2008;137(2):57–81.
[167] Zhou Q, Sun Y, Yi S, Wang K, Luo G. Investigation of droplet coalescence in nanoparticle suspensions by a microfluidic collision experiment. Soft Matter 2016;12(6):1674–82.
[168] Alvarez NJ, Anna SL, Saigal T, Tilton RD, Walker LM. Interfacial dynamics and rheology of polymer-grafted nanoparticles at air-water and xylene–water interfaces. Langmuir. 2012;28(21):8052–63.
[169] Gunes DZ, Bercy M, Watzke B, Breton O, Burbidge AS. A study of extensional flow induced coalescence in microfluidic geometries with lateral channels. Soft Matter 2013;9(31):7526–37.
[170] Bremond N, Thiam AR, Bibette J. Decompressing emulsion droplets favors coalescence. Phys Rev Lett 2008;100(2):024501.
[171] Christopher G, Bergstein J, End N, Poon M, Nguyen C, Anna SL. Coalescence and splitting of confined droplets at microfluidic junctions. Lab Chip 2009;9(8): 1102–9.
[172] Jose BM, Cubaud T. Droplet arrangement and coalescence in diverging/ converging microchannels. Microfluid Nanofluid 2012;12(5):687–96.
[173] Baret J-C, Kleinschmidt F, El Harrak A, Griffiths AD. Kinetic aspects of emulsion stabilization by surfactants: a microfluidic analysis. Langmuir. 2009;25(11): 6088–93.
[174] Krebs T, Schroen K, Boom R. A microfluidic method to study demulsification kinetics. Lab Chip 2012;12(6):1060–70.
[175] Krebs T, Schroën C, Boom R. Coalescence kinetics of oil-in-water emulsions studied with microfluidics. Fuel. 2013;106:327–34.
[176] Krebs T, Schroen C, Boom R. A microfluidic study of oil-water separation kinetics. Adv Fluid Mech IX 2012;74:427–38.
[177] Krebs T, Schroën K, Boom R. Coalescence dynamics of surfactant-stabilized emulsions studied with microfluidics. Soft Matter 2012;8(41):10650–7.
[178] Muijlwijk K, Colijn I, Harsono H, Krebs T, Berton-Carabin C, Schroën K. Coalescence of protein-stabilised emulsions studied with microfluidics. Food Hydrocoll 2017;70:96–104.
[179] Dudek M, Fernandes D, Herø EH, Øye G. Microfluidic method for determining drop-drop coalescence and contact times in flow. Colloids Surf A Physicochem Eng Asp 2020;586:124265.
[180] Abedi S, Suteria NS, Chen C-C, Vanapalli SA. Microfluidic production of size-tunable hexadecane-in-water emulsions: effect of droplet size on destabilization of two-dimensional emulsions due to partial coalescence. J Colloid Interface Sci 2019;533:59–70.
[181] Kovalchuk NM, Roumpea E, Nowak E, Chinaud M, Angeli P, Simmons MJ. Effect of surfactant on emulsification in microchannels. Chem Eng Sci 2018;176: 139–52.
[182] Kole S, Bikkina P. A parametric study on the application of microfluidics for emulsion characterization. J Pet Sci Eng 2017;158:152–9.
[183] Schröder A, Sprakel J, Schroën K, Spaen JN, Berton-Carabin CC. Coalescence stability of Pickering emulsions produced with lipid particles: a microfluidic study. J Food Eng 2018;234:63–72.
[184] Yao X, Liu Z, Ma M, Chao Y, Gao Y, Kong T. Control of particle adsorption for stability of Pickering emulsions in microfluidics. Small. 2018;14(37):1802902.
[185] Mulligan MK, Rothstein JP. Deformation and breakup of micro-and nanoparticle stabilized droplets in microfluidic extensional flows. Langmuir. 2011;27(16): 9760–8.
[186] Sun J, Wang W, He F, Chen Z-H, Xie R, Ju X-J, et al. On-chip thermo-triggered coalescence of controllable Pickering emulsion droplet pairs. RSC Adv 2016;6 (69):64182–92.
[187] Priest C, Reid MD, Whitby CP. Formation and stability of nanoparticle-stabilised oil-in-water emulsions in a microfluidic chip. J Colloid Interface Sci 2011;363(1): 301–6.
[188] Xu B, Nguyen N-T, Wong TN. Temperature-induced droplet coalescence in microchannels. Biomicrofluidics. 2012;6(1):012811.
[189] Luong T-D, Nguyen N-T, Sposito A. Thermocoalescence of microdroplets in a microfluidic chamber. Appl Phys Lett 2012;100(25):254105.
[190] Lai A, Bremond N, Stone HA. Separation-driven coalescence of droplets: an analytical criterion for the approach to contact. J Fluid Mech 2009;632:97–107.
[191] Gunes DZ, Clain X, Breton O, Mayor G, Burbidge AS. Avalanches of coalescence events and local extensional flows–stabilisation or destabilisation due to surfactant. J Colloid Interface Sci 2010;343(1):79–86.
[192] Gunes DZ, Clain X, Burbidge AS. Evidence of droplet coalescence in extensional flow using microfluidic devices. AIP Conf Proc 2008;1027:878–80.
[193] Malcolm AS, Dexter AF, Katakdhond JA, Karakashev SI, Nguyen AV, Middelberg AP. Tuneable control of interfacial rheology and emulsion coalescence. ChemPhysChem. 2009;10(5):778–81.
[194] Bauer W-AC, Kotar J, Cicuta P, Woodward RT, Weaver JV, Huck WT. Microfluidic production of monodisperse functional O/W droplets and study of their reversible pH dependent aggregation behavior. Soft Matter 2011;7(9):4214–20.
[195] Yoon Y, Baldessari F, Ceniceros HD, Leal LG. Coalescence of two equal-sized deformable drops in an axisymmetric flow. Phys Fluids 2007;19(10):102102.
[196] Williams YON, Roas-Escalona N, Rodríguez-Lopez G, Villa-Torrealba A, Toro-Mendoza J. Modeling droplet coalescence kinetics in microfluidic devices using population balances. Chem Eng Sci 2019;201:475–83.
[197] Chen D, Cardinaels R, Moldenaers P. Effect of confinement on droplet coalescence in shear flow. Langmuir. 2009;25(22):12885–93.
[198] Shenoy A, Rao CV, Schroeder CM. Stokes trap for multiplexed particle manipulation and assembly using fluidics. Proc Natl Acad Sci 2016;113(15): 3976–81.
[199] Kuma D. A microfluidic device for producing controlled collisions between two soft particles.. Master Thesis. Canada: Department of Chemical Engineering and Applied Chemistry, University of Toronto; 2016.
[200] Krebs T, Ershov D, Schroen C, Boom R. Coalescence and compression in centrifuged emulsions studied with in situ optical microscopy. Soft Matter 2013;9 (15):4026–35.
[201] Feng H, Ershov D, Krebs T, Schroen K, Stuart MAC, van der Gucht J, et al. Manipulating and quantifying temperature-triggered coalescence with microcentrifugation. Lab Chip 2015;15(1):188–94.
[202] Goel S, Ng S, Acosta E, Ramachandran A. The roles of contact time and contact pressure on the coalescence of water droplets suspended in concentrated bitumen solutions. Fuel. 2018;223:486–95.